VŠB – Technical University of Ostrava

# Lattice dynamics of actinides and actinide compounds from first-principles calculations

# Dynamika atomové mříže aktinidů a aktinidiových sloučenin – výpočty z prvních principů

2018

Author: Bc. Lukáš Kývala
Supervisor: Ing. Dominik Legut Ph.D.

VŠB - Technical University of Ostrava
University Study Programmes
IT4Innovations

# Bachelor Thesis Assignment

| | |
|---|---|
| Student: | **Bc. Lukáš Kývala** |
| Study Programme: | B3942 Nanotechnology |
| Study Branch: | 3942R001 Nanotechnology |
| Title: | Lattice dynamics of actinides and actinide compounds from first-principles calculations<br>Dynamika atomové mříže aktinidů a aktinidiových sloučenin - výpočty z prvních principů |
| The thesis language: | English |

Description:

The actinide carbides can be used as advanced nuclear fuels for the so-called generation IV reactors (including the gas-cooled and sodium-cooled fast reactors). These carbides are promising because of higher thermal conductivity and operational temperature (more efficient heat transfer) over conventional oxide fuels (e.g. UO2). The actinides pose 5f electrons, which are crucial for electronic structure and lattice dynamics. The primary goal is to investigate the effect of spin-orbit interactions, the influence of the localization of 5f electrons on the electronic structures of actinides and actinide carbides within density functional theory. Next the lattice dynamics (phonons) are to be calculated within the quasi-harmonic approximation and subsequently a determination of the thermal expansion, phase stability and other thermodynamical properties. Finally the results are to be compared with experimental data.

References:

1. Introduction to solid state physics, Charles Kittel, John Wiley & sons (1996).
2. R. M. Martin, Electronic Structure: Basic Theory and Practical Methods, Cambridge University Press 2004.
3. N. Ashcroft, N. Mermin, Solid State Physics, Cengage Learning 1976.
4. E. Kaxiras, Atomic and Electronic Structure of Solids, Cambridge University Press 2003.
5. Principles of Condensed Matter Physics, P. M. Chaikin, T. C. Lubensky, Cambridge Press (2000).
6. Band Theory and Electronic Properties of Solids, J. Singleton, Oxford Master Series in Physics (2001).
7. Magnetism in Condensed Matter, S. Blundell, Oxford Master Series in Physics (2001).

Extent and terms of a thesis are specified in directions for its elaboration that are opened to the public on the web sites of the faculty.

Supervisor: **Ing. Dominik Legut, Ph.D.**

Date of issue: 24.11.2017

Date of submission: 21.05.2018

doc. Mgr. Vít Vondrák, Ph.D.
*Head of Department*

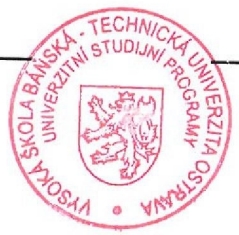


Ing. Zdeňka Chmelíková, Ph.D.
*Vice-rectress for Study Affairs*

Prohlašuji, že jsem tuto bakalářskou práci vypracoval samostatně. Uvedl jsem všechny literární prameny a publikace, ze kterých jsem čerpal.

Ostrava, 21. května 2018 .....

## Prohlášení o využití výsledků práce

- Byl jsem seznámen s tím, že na moji bakalářskou práci se plně vztahuje zákon č.121/2000Sb., autorský zákon, zejména §35 – užití díla v rámci občanských a náboženských obřadů, v rámci školních představení a užití díla školního a §60 – školní dílo.
- Beru na vědomí, že Vysoká škola báňská – Technická univerzita Ostrava (dále jen VŠB-TUO) má právo nevýdělečně ke své vnitřní potřebě bakalářskou práci užít (§35 odst. 3).
- Souhlasím s tím, že bakalářská práce bude v elektronické podobě uložena v Ústřední knihovně VŠB-TUO k nahlédnutí a jeden výtisk bude uložen u vedoucího bakalářské práce. Souhlasím s tím, že údaje o bakalářské práci budou zveřejněny v informačním systému VŠB-TUO.
- Bylo sjednáno, že s VŠB-TUO, v případě zájmu z její strany, uzavřu licenční smlouvu s oprávněním užít dílo v rozsahu §12 odst. 4 autorského zákona.
- Bylo sjednáno, že užít své dílo - bakalářskou práci - nebo poskytnout licenci k jejímu využití mohu jen se souhlasem VŠB-TUO, která je oprávněna v takovém případě ode mne požadovat přiměřený příspěvek na úhradu nákladů, které byly VŠB-TUO na vytvoření díla vynaloženy (až do jejich skutečné výše).
- Beru na vědomí, že odevzdáním své práce souhlasím se zveřejněním své práce podle zákona č. 111/1998 Sb., o vysokých školách a o změně a doplnění dalších zákonů (zákon o vysokých školách), ve znění pozdějších předpisů, bez ohledu na výsledek její obhajoby.

Bc. Lukáš Kývala, Nižní Lhoty 47, 739 51 Nižní Lhoty

Ostrava, 21. května 2018 .....

Rád bych poděkoval Ing. Dominiku Legutovi Ph.D. za odborné rady a věcné připomínky, které mi poskytl při zpracování této práce.

**Abstrakt**

Aktinidy jsou první prvky z periodické tabulky, které obsahují $5f$ elektrony. $5f$ elektrony jsou unikátní díky jejich schopnosti být zároveň částečně lokalizované a delokalizované. Vzájemný podíl lokalizovaných a delokalizovaných $5f$-stavů výrazně ovlivňuje výsledné vlastnosti materiálu, a proto jeho přesné určení je nutné. Také spin-orbitální interakce může hrát významnou roli pro tyto prvky s vysokým atomovým číslem díky nárůstu vlivu relativistických efektů. Díky dobře nastavené lokalizaci $5f$-stavů skrze Hubbard $U$ korekci a zahrnutí spin-orbitální interakce, jsou v této práci reprodukovány elektronové, mechanické, fononové a termodynamické vlastnosti kovového thoria a monokarbidu thoria. Zároveň jsou předpovězeny elektronové, mechanické, fononové a termodynamické vlastnosti monokarbidu protaktinia, u kterého je experimentálně známa pouze mřížková konstanta. Výzkum obou monokarbidů je nutný z důvodu jejich potenciálu stát se budoucími jadernými palivy. Vliv zahrnutí spin-orbitální interakce a lokalizace $5f$-stavů je v práci diskutován nejen na základě porovnání s experimenty, ale také na základě porovnání s ostatními teoretickými pracemi.

**Klíčová slova**: ab initio, výpočty z prvních principů, thorium, protactinium, mechanika, termodynamika, fonony, jaderná paliva

**Abstract**

Actinides are the first elements of a periodic table that contain $5f$ electrons. $5f$ electrons are unique due to their ability to be partially localized and delocalized. The ratio of localization and delocalization of $5f$-states significantly affects the resulting material properties and therefore its exact determination is necessary. Also, spin-orbital interactions can play a significant role for high atomic number elements due to the increase of relativistic phenomena. Based on the well-determined localization of $5f$-states through Hubbard $U$ correction and the inclusion of spin-orbital interaction, the electron, mechanical, phonon and thermodynamic properties of thorium metal and thorium monocarbide are reproduced in this work. At the same time, the electron, mechanical, phonon and thermodynamic properties of the protactinium monocarbide are predicted because only a lattice constant being known experimentally. Research on both monocarbides is necessary because of their potential to become future nuclear fuels. The influence of the spin-orbital interaction and localization of $5f$-states is discussed not only on the basis of comparison with experiments but also on comparison with other theoretical works.

**Key Words**: ab initio, calculations from first principles, thorium, protactinium, mechanical, thermodynamics, phonons, nuclear fuels

# Contents

## List of abbreviations

| | | |
|---|---|---|
| APW | – | Augmented Plane Wave method |
| BIS | – | Bremsstrahlung Isochromat Spectroscopy |
| DFT | – | Density Functional Theory |
| FLAPW | – | Full-potential Linear Augmented Plane-Wave method |
| GGA | – | Generalized Gradient Approximations |
| LDA | – | Local Density Approximation |
| PAW | – | Projector Augmented Wave |
| PBE | – | Perdew-Burke-Ernzerhof exchange correlation functional |
| PBEsol | – | Perdew-Burke-Ernzerhof exchange correlation functional for solids |
| QHA | – | Quasi-Harmonic Approximation |
| SOI | – | Spin-Orbit Interaction |
| UPS | – | Ultraviolet Photoelectron Spectroscopy |
| VASP | – | Vienna Ab initio Simulation Package |
| XPS | – | X-ray Photoelectron Spectroscopy |

# List of Figures

## List of Tables

# 1 Introduction

The theoretical investigation of material properties gains popularity among a wide range of researchers. Computational material science is as accessible as ever before because of sophisticated mathematical approaches and available computational power. This allows scientists to discover the background of processes that are not easily detectable from experimental measurements.

However, the exact solution of the Schrödinger equation is still an impossible task. Many approximations must be applied to achieve a feasible calculation. Some are reasonable and preserve the accuracy of the results but some bring inaccuracies and researchers have to keep them in mind. Moreover, calculations are solved numerically, so it is necessary to deal with numerical precision.

There are many approaches with variously applied approximations and implemented techniques nowadays. While two different approaches can provide the results with the necessary precision, the computational resources used can be quite different. Therefore, it is necessary to know which approach is appropriate for the situation and the system. The balance between accuracy and computational requirements is always required.

Theoretical calculations in material sciences are used to predict a vast array of properties, such as electronic, mechanical, magnetic, optical, phonon, thermodynamic, and even superconducting. This thesis focuses on electronic, mechanical, phonon and thermodynamic properties of possible future nuclear fuels.

Nuclear fuels are a characteristic case where the usefulness of theoretical research is demonstrated. While the experimenters have a difficult task to work with these materials because of high radioactivity, this radioactivity does not concern theoreticians.

Theoretical investigations can not only provide missing information but also predict properties under precisely defined conditions. Different stoichiometry, pressure, temperature, impurities are a solvable task for a theoretical calculation.

# 2 Theory

## 2.1 Actinides

The actinide elements are the 15 chemical elements with atomic numbers 89 through 103, the first member of which is actinium and the last member is lawrencium. The electron configuration of actinides is $1s^2\ 2s^2\ 2p^6\ 3s^2\ 3p^6\ 3d^{10}\ 4s^2\ 4p^6\ 4d^{10}\ 5s^2\ 5p^6\ 4f^{14}\ 5d^{10}\ 6s^2\ 6p^6$. Outer electrons may be accommodated in the $5f$, $6p$ and $7s$ shells as it comes out of the quantum treatment of the hydrogenoid atom [1].

Occupied $5f$ states and atomic nuclei with many protons cause a great variety of unique properties. Among the most unique belong:

- All elements heavier than uranium were first discovered by bombardment of heavy atoms with neutrons in nuclear reactors, bombardment with other particles in accelerators, or as the result of nuclear detonations.
- All actinide isotopes are radioactive.
- In all forms (metal, chemical compounds and in solution) have very large radii.
- Their metals manifest an unusual range of physical properties. For example, plutonium has six allotropes [2].

### 2.1.1 5*f*-electrons and their dual nature

Generally, electrons can be divided into localized and itinerant. Itinerant electrons give rise to metallic character. Metallic behavior is advantageous because of the saving of kinetic energy due to delocalization over the whole of a crystal [3]. But if on-site Coulomb energy (the cost of putting two electrons on the same lattice site) is strong enough, electrons cannot move freely through the crystal and electron-electron correlations at a given lattice site become large enough to prevent those electrons from hopping between sites and electrons remain localized [4].

The radial probability of finding an electron at a distance $\vec{r}$ from the nucleus is shown for the valence $4f$, $5d$, $6s$, and $6p$ orbitals of $Sm^{3+}$ in Appendix. It suggests that because of the small radial part of the $4f$ wavefunction, $4f$ electrons are able to appreciably penetrate the xenon core. Because of being shielded by the $5s^2$ and $5p^6$ orbitals, they cannot overlap with ligand orbitals and hence do not contribute to the cohesion of the solid. Therefore the electronic bonding of lanthanides is provided only by two or three conduction-band electrons [4, 5].

The nature of $5f$ electrons differs from $4f$ electrons. The $5f$ electron distribution extends out much farther from the nucleus than a $4f$ electron does as shown in Appendix [6]. While $4f$ states are primarily localized, a part of *5f-states* is delocalized and contributes to chemical bonding. The dual nature of $5f$ electrons is supported by a great variety of experiments including, e. g., photoemission and neutron inelastic scattering as well as muon spin relaxation measurement [7].

Delocalization of $5f$ states arises from the interplay between the hybridization of the $5f$ states with the conduction electrons, and because $5f$ electrons see their own centrifugal potential, due to their high angular momentum (l = 3). Thus, the $5f$ electrons can tunnel the potential barrier to the next ion but such hopping costs Coulomb energy (Hubbard $U$). If on-site Coulomb interaction is large, $5f$ electrons appear to be localized in the ground state [1].

From the electronic structure point of view, this results in part of the $5f$-*states* being found in dispersive and hybridized bands in the vicinity of the Fermi level, whereas the second part of $5f$ electrons remains localized [8].

For example, theoretical calculation of $\delta$-Pu provides very good agreement with measured photoemission spectrum and indicates that the electronic structure of $\delta$-Pu involves four localized $5f$ electrons and approximately one $5f$ electron forming an itinerant band located at the Fermi level [8].

Accurate determination of the ratio between itinerant or localized behavior is very important because many of the fundamental properties of the actinides depend on the properties of the $5f$ electrons and on the question of whether those electrons are localized or delocalized [4]. Moreover, this determination is complicated because behavior of itinerant or localized states depends on conditions such as temperature and applied pressure [2].

### 2.1.2 Magnetism

An atom containing an unsaturated inner shell displays a net magnetic moment. Because of that magnetism is found in transition metal atoms (unfilled $d$ shell), in lanthanides (unfilled $4f$ shell) and in actinides (unfilled $5f$ shell). The magnetic moment is caused by the fact that the electrons adhere to the Hund's rules and fill the shell in such a way as to have the maximum alignment of their spins [1].

The magnetic properties of actinide compounds are difficult to interpret since it is not clear whether non-fully localized $5f$ electron states should be described in a localized or an itinerant picture.

Experiments have shown that all the light actinides are paramagnetic. Spontaneously order in a magnetic configuration does not occur even at the very lowest temperatures. Only when an external magnetic field is applied, small (positive) magnetic moment appears. This finding is consistent with the fact that the $5f$ electrons in the light actinides are of delocalized rather than localized nature [4], because *f-f*-overlapping is so large that $5f$-bands become broad bands and only the typical weak Pauli paramagnetism of free electrons is found in the presence of an external magnetic moment [1].

The various magnetic properties observed in actinide solids are largely determined by the degree the unsaturated $5f$ shells retain an atomic localized character or lose it in an itinerant mode [1].

### 2.1.3 Thorium

Thorium (Th), the second actinide element, is weakly radioactive silvery metal with atomic number 90. Thorium holds the face-centered cubic (*fcc*) structure (space group $Fm\bar{3}m$, No. 225) at ambient conditions and exhibits only Pauli paramagnetism [9] due to *f*-*f*-overlapping [1].

Common applications of thorium compounds include incandescent gas mantles, a production of ceramics, carbon arc lamps, coating for tungsten welding rods, additive into a refractive glass, heat-resistant laboratory crucibles and can also be used as a catalyst [2].

However, current attention paid to this element is due to possible use as nuclear fuels in Generation IV nuclear reactors [10]. Thorium is 3 to 4 more abundant than uranium while widely distributed in nature as an easily exploitable resource in many countries. Unlike uranium where it is necessary to distinguish 'fissile' $^{235}$U isotope and $^{233}$U isotope, thorium can be found only in 'fertile' $^{232}$Th isotope. Moreover, thorium fuel cycle produces less radiotoxicity waste than uranium fuel cycle [11].

From thorium position in the periodic table could be assumed that thorium should hold hexagonal close-packed (hcp) crystal structure as others in group IVA elements (Ti, Zr and Hf). But among these tetravalent elements, thorium is the only one element in the group, which holds the *fcc* crystal structure. This anomaly is attributed to the presence of 5*f*-states involved in chemical bonds [12].

Without occupation of 5*f*-states, thorium would hold body-centered cubic (bcc) crystal structure and would exhibit normal tetravalent *d* metal behavior as in the case of Ti, Zr and Hf. Only when the 5*f*-states occupation is taken into account, the *fcc* structure becomes the ground-state structure in agreement with experiments [12].

### 2.1.4 Protactinium

Protactinium (Pa), the third actinide element and the first having a $5f$ electron in an isolated atom, is silvery-gray metal with atomic number 91. Since the half-time of the most stable isotope $^{231}$Pa is short in geological terms, protactinium is one of the most rarest of the naturally occurring elements and one of the most difficult of all to extract from natural sources because its natural occurrence is closely tied to $^{235}$U, its primordial ancestor, which is widely distributed in the Earth's crust [2].

Protactinium holds the body-centered tetragonal (bct) structure (space group I4/mmm, No. 139) at ambient conditions and exhibits only Pauli paramagnetism [2] due to *f*-*f*-overlapping [1] as in the case of thorium.

Protactinium is used for the preparation of a scintillator for detecting X-rays and as a dopant to mixed oxides of Nb, Mg, Ga and Mn for production high-temperature dielectrics (up to 1300 °C) used as ceramic capacitors. Protactinium can also be used in the determination of ancient subjects using a $^{231}$Pa/$^{235}$U dating method [2].

The most important application is not based on the most stable $^{231}$Pa isotope but on $^{233}$Pa which is an intermediate in the production of fissile $^{231}$U in thorium breeder reactors.

### 2.1.5 Carbides

Carbides are chemical compounds in which carbon bonds with less electronegative elements. Based on differences in electronegativity and the valence state of the constituting elements, monocarbides can be divided according to the type of bond:

- salt-like compounds (carbon with highly electropositive elements),
- covalent compounds (e. g. SiC),
- interstitial compounds (carbon with transition metals of the group 4, 5 and 6 transition metals except for chromium),
- intermediate transition metal carbides [13].

Actinides form three types of stoichiometric carbides – monocarbides (AnC), dicarbides ($AnC_2$) and sesquicarbides ($An_2C_3$). Monocarbides and dicarbides can be found for protactinium, thorium, uranium, neptunium and plutonium. Sesquicarbides have been observed for thorium, uranium, neptunium, plutonium, americium and curium [13].

Actinide carbides are described as salt-like type. However, chemical bonding is more complicated. Ionic bonding is present due to the electronegativity difference between the actinide and the non-actinide element. Actinide carbides are metals, therefore metallic bonding is also involved. Covalent part in the bonding is derived from hybridization not only with the other outer actinide electronic orbitals (especially the $6d$) but also with the outer electronic orbitals of the non-actinide element. As a result, metallic, covalent, and ionic bonds take place in actinides carbides [13].

Monocarbides, which are investigated in this thesis, crystallize in NaCl-type space group $Fm\overline{3}m$, No. 225. The atom distribution of NaCl-type space group is shown in Fig 1. The lattice parameter depends on the C/An ratio, and the amount of oxygen and nitrogen impurities which are always present.

The beginning of the research on actinide carbides as a nuclear fuel dates back to the 1950s. Then, because the option of fast reactors for civilian purposes was forbidden, uranium dioxide and mixed uranium-plutonium oxides began to prevail as nuclear fuel in most of Generation II and III power plants. As a result, research has not been done for carbides until the 1990s. In the last years, interest has been renewed because carbides are one of the possible nuclear fuel of Generation IV nuclear systems development [10].

Carbides are more suitable as nuclear fuel than oxides because of higher burnup, higher density, higher temperature operation, higher thermal conductivity, and better compatibility with clad materials [13, 14].

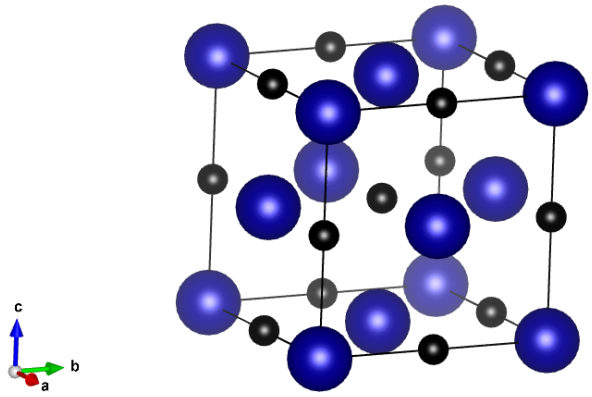


Figure 1: The unit cell of actinide monocarbide (AnC). Blue spheres represent actinide atoms, and black ones are carbon atoms.

Investigated thorium carbides can be used as fertile material in breeder reactors where the only natural $^{232}$Th isotope absorbs a thermal neutron to produce fissile $^{233}$U. Obstruction to the implementation of this cycle is $^{232}$Pa, which is formed as an intermediate in the conversion chain of $^{232}$Th to $^{233}$U and has relatively long half-time (27 days) [11].

Nowadays, the thorium fuel cycle is mostly investigated in India, which has about one-fourth of the total world thorium resources, but this option is also considered by other countries with thorium supplies (Norway, Australia, USA, China, Canada *etc.*) [1].

## 2.2 Density Functional Theory

### 2.2.1 Quantum theory of electrons in solids

All measurable properties of all forms of matter are determined completely by quantum mechanics from solutions of the time-dependent many-body Schrödinger equation for the motion of the electrons and the nuclei. The properties are divided into equilibrium and nonequilibrium (response). Equilibrium properties determine all thermodynamic behavior like the equations of state, heat capacities, thermal expansion *etc.* Nonequilibrium properties encompass responses to various perturbations (mechanical force and electromagnetic fields) and result in the mechanical, transport, and optical properties of materials.

Nevertheless, the solution of a time-dependent many-body Schrödinger equation for the motion of the electrons and the nuclei is impossible. Many approximations must be applied to obtain at least an approximate solution [15].

### 2.2.2 Non-relativistic Schrödinger equation

To find the properties of solids, the time-dependent many-body Schrödinger equation must be solved:

$$\hat{H}\Psi(\{\vec{r_i}\},\{\vec{R_\alpha}\},t) = i\hbar\frac{\partial\Psi}{\partial t} \tag{1}$$

where H is the exact many-body Hamiltonian and $\Psi$ is the wavefunction of the all electronic and nuclear coordinates, which are detonated by $\vec{r_i}$ and $\vec{R_\alpha}$. This equation cannot be solved because the common solid contains $10^{25}$-$10^{26}$ electrons and $10^{24}$ nuclei interacting with each other. Because under normal conditions the speed of electrons ($v_i$) or cores ($V_\alpha$) is not anywhere near the speed of light, first non-relativistic approximation is made:

$$\hat{H} = \sum_i \frac{\vec{p_i^2}}{2m} + \sum_\alpha \frac{\vec{P_\alpha^2}}{2M_\alpha} + \frac{1}{2}{\sum_{i,j}}' \frac{e^2}{|\vec{r_i}-\vec{r_j}|} + \frac{1}{2}{\sum_{\alpha,\beta}}' \frac{Z_\alpha Z_\beta e^2}{|\vec{R_\alpha}-\vec{R_\beta}|} - \sum_{i,\alpha}\frac{Z_\alpha e^2}{|\vec{r_i}-\vec{R_\alpha}|} \tag{2}$$

where $\vec{p_i}$ and $\vec{P_\alpha}$ are the momenta of the electrons and ion cores, $m$ and $M_\alpha$ are the mass of the electron and ion core and $Z_\alpha$ is the charge of that ion core. The terms with the momenta of the electrons and ion cores represent kinetic energy. Next terms represent the repulsive Coulomb interaction potential energy between electrons and ion cores. Both are divided by two because interactions between $i$ and $j$ are the same as $j$ and $i$. The last term represents the attractive Coulomb potential energy between the electrons and the ion cores.

This Hamiltonian omits relativistic corrections as spin-orbit coupling, magnetic effects and mass-velocity effects. However, solving this equation is still an impossible task. Further approximations are required [15].

### 2.2.3 Adiabatic Approximation

Even the lightest atomic nucleus is about 1800x heavier than an electron. From the first two members of the Eq. 1, it could be considered that nucleus moves much more slowly than the electron and hence the nucleus does not move in the frame of the electron [16].

This allows the separation of variables and the wavefunction of the whole system can then be broken down into the wavefunction depending only on electrons coordinates ($\Phi$) with fixed set of ion-core positions $\vec{R_\alpha}$ and wavefunction depending only on ion cores coordinates ($\psi$):

$$\Psi(\{\vec{r_i}\},\{\vec{R_\alpha}\}) = \Phi(\{\vec{r_i}\},\{\vec{R_\alpha}\})\,\psi(\{\vec{R_\alpha}\}) \tag{3}$$

The time-dependent solution will then be:

$$\Psi(\{\vec{r_i}\},\{\vec{R_\alpha}\},t) = \Phi(\{\vec{r_i}\},\{\vec{R_\alpha}\})\,\psi(\{\vec{R_\alpha}\})\,e^{-\frac{iEt}{\hbar}} \tag{4}$$

Substituting this equation into Eq. 1-2, the original equation is divided into Schrödinger equation as the function of electron coordinates ($\Phi$) and Schrödinger equation as the function of ion cores coordinates ($\psi$). The electronic Schrödinger equation ($\Phi$) is:

$$\left(\sum_i \frac{\vec{p_i^2}}{2m} + \frac{1}{2}{\sum_{i,j}}' \frac{e^2}{|\vec{r_i}-\vec{r_j}|} - \sum_{i,\alpha}\frac{Z_\alpha e^2}{|\vec{r_i}-\vec{R_\alpha}|}\right)\Phi_n = E_n\Phi_n \tag{5}$$

Solving this equation yields the eigenvalues $E_n(\vec{R_\alpha})$ and the eigenfunctions $\Phi(\{\vec{r_i}\},\{\vec{R_\alpha}\})$ for a fixed set of ion-core positions $\vec{R_\alpha}$.

For ion cores wavefunction ($\psi$) is:

$$\left(\sum_\alpha \frac{\vec{P_\alpha^2}}{2M_\alpha} + \frac{1}{2}{\sum_{\alpha,\beta}}' \frac{Z_\alpha Z_\beta e^2}{|\vec{R_\alpha}-\vec{R_\beta}|} + E_n(\{\vec{R_\alpha}\})\right)\psi_{n,\lambda} = E_{n,\lambda}\psi_{n,\lambda} \tag{6}$$

The electronic coordinates do not explicitly enter this equation but enter implicitly through the term $E_n(\vec{R_\alpha})$ as potential energy. Since, for each $n$, the $E_n(\vec{R_\alpha})$ member will acquire a different value and therefore different eigenvalues $E_{n,\lambda}$ and eigenfunctions $\Psi_{n,\lambda}$ are obtained [15].

### 2.2.4 Hartree Approximation

The electronic wavefunction from Eq. 5 can be written as a product of wavefunctions $\phi$ for each particle (electron) $n$ in the system:

$$\Phi(\{\vec{r_i}\}) = \phi_1(\vec{r}_1)\phi_2(\vec{r}_2)...\phi_n(\vec{r}_n) \tag{7}$$

From the point of view of probability theory, this equation states that the motion of each particle $n$ is independent. It does not mean that they do not interact, but it assumes that the electron interacts only with the effective field generated by the other electrons [16].

A solution of the Schrödinger equation, which is based on a variables principle, minimizes the energy of the Hamiltonian in Eq. 5 depending on the changes in $\phi_i$. Each particle $n$ has their own effective Schrödinger equation $\phi_i$:

$$\left(-\frac{\hbar^2}{2m}\nabla_i^2 + e^2\sum_{j\neq i}\int\frac{|\phi_j(\vec{r})|^2}{|\vec{r_i}-\vec{r}|}\vec{dr} - e^2\sum_{\alpha}\frac{Z_\alpha}{|\vec{r_i}-\vec{R_\alpha}|}\right)\phi_i(\vec{r_i}) = \epsilon\phi_i(\vec{r_i}) \tag{8}$$

The first term represents kinetic energy, the second term represents the Coulomb potential generated by all the other electrons and the last one represents attractive Coulomb potential generated by the ion cores.

This process solutions to the Schrödinger equation is known as Hartree approximation and has one big drawback. It does not respect the antisymmetric statistics of electrons and therefore drastically underestimates the tendency for cohesion due to excess of repulsive Coulomb interaction [15].

### 2.2.5 Hartree-Fock Approximation

Since the wavefunction must respect the antisymmetric symmetry of the electrons, instead of Eq. 7, the wavefunction must be written in form of a Slater determinant:

$$\Phi(\{\vec{r_i}\}) = \frac{1}{\sqrt{n!}}\begin{vmatrix} \phi_1(\vec{r}_1) & \phi_2(\vec{r}_2) & \cdots\ \phi_1(\vec{r}_n) \\ \phi_2(\vec{r}_1) & \phi_2(\vec{r}_2) & ... & \vdots \\ \vdots & \vdots & \ddots & \vdots \\ \phi_n(\vec{r}_1) & \cdots & \cdots\ \phi_n(\vec{r}_n) \end{vmatrix} \tag{9}$$

The expression of the wavefunction in the form of the Slater determinant changes the effective Schrödinger equation (Eq. 8) to:

$$\left(-\frac{\hbar^2}{2m}\nabla_i^2 + e^2\sum_{j\neq i}\int\frac{|\phi_j(\vec{r})|^2}{|\vec{r_i}-\vec{r}|}\vec{dr} - e^2\sum_{\alpha}\frac{Z_\alpha}{|\vec{r_i}-\vec{R_\alpha}|}\right)\phi_i(\vec{r_i}) - e^2\sum_{j}\int\frac{\phi_j^*(\vec{r})\phi_j(\vec{r})\phi_i(\vec{r})}{|\vec{r_i}-\vec{r_j}|}\vec{dr_j} = \epsilon\phi_i(\vec{r_i}) \tag{10}$$

The first three terms are the same as those of the Hartree approximation. There is now a fourth member who represents the Pauli exclusion principle and is called the exchange term. This term has negative sign because the overlap of spatial wavefunctions with the same spin is minimized and therefore repulsive Coulomb interaction is reduced. It stabilizes the system by increasing cohesive energy of solids.

But treating parallel spins apart is not enough, the same effect for electrons with anti-parallel is also needed, because otherwise tendency toward cohesion is underestimated. This

type of treating is not included in antisymmetrization of the wavefunction and must be achieved in a different way. The difference between the exact energy of a system and the energy calculated in the Hartree-Fock approximation is called the correlation energy, where all electron-electron interactions that go beyond the classical Hartree term are found [15].

### 2.2.6 Basic Density Functional Theory

Density Functional Theory (DFT) is the predominant method for calculating the electron structure nowadays. The success of the DFT is based on the fact that it provides a balance between accuracy and calculation costs. This makes it possible to calculate much larger systems with very good accuracy while traditional wavefunction methods, either variational or perturbative, can be used for highly accurate results on smaller systems or provide a comparison to the accuracy of the DFT [17].

The Density Functional Theory is based on two theorems. Based on the first theory, this theory was named. This theorem states:

*The total energy E of a quantum mechanical system depends only on the electron density $\rho$ of its ground state, i. e., energy E is functional, which assigns a number to a function, of the electron density $\rho$.*

$$E = E[\rho(\vec{r})] \tag{11}$$

and the ground state energy can be found in minimum:

$$\left.\frac{\partial E[\rho]}{\partial \rho}\right|_{\rho_0} = 0 \tag{12}$$

where $\rho_0$ is the exact electron density of the many-body ground state [15].

Let's specify what exactly is the electron density. Electron density, unlike the wavefunction, is of direct physical significance. It is the probability of finding an electron in some space.

However, it is important to keep in mind that the electron density is not the same as the square of the wavefunction in absolute value because the square of the wavefunction gives us the probability of finding the given electron having the specified spin in some space. It gives us information about all the electrons, so the number of degrees of freedom is 4N where N is around $10^{24}$ while electron density is a scalar function and depends only on 3 variables [16].

Electronic density is related to the wavefunction of the system according to the relationship:

$$\rho = N \int |\psi(\vec{r}_1, \vec{r}_2, ..., \vec{r}_n)|^2 d\vec{r}_2 ... d\vec{r}_n \tag{13}$$

If the electron density is integrated across the whole space, the number of electrons in the system is obtained [16]:

$$\int \rho d\vec{r} = N \tag{14}$$

Since the electron density is also given by the position of the nucleus, the Eq. 11 is overwritten:

$$E = E[\rho(\vec{r}, \{\vec{R_\alpha}\})] \tag{15}$$

where $\vec{R_\alpha}$ are sets of fixed ion-core positions and therefore it is more as a parameter than a degree of freedom.

The second theorem is based on the idea that each electron moves independently ("effective electron") at the average effective potential $V_{eff}$ that is generated by the other electrons and the core. This potential must be found self-consistently because the wavefunction of each electron is involved in the effective potential of all other electrons.

The Schrödinger equation of effective electrons:

$$\left(-\frac{\hbar^2}{2m}\nabla^2 + V_{eff}\right)\psi_i(\vec{r}) = \epsilon_i\psi_i(\vec{r}) \tag{16}$$

where the effective potential is given by:

$$V_{eff}(\vec{r}) = e^2\int\frac{\rho(\vec{r'})}{|\vec{r}-\vec{r'}|}\vec{dr} - e^2\sum_\alpha\frac{Z_\alpha}{|\vec{R_\alpha}-\vec{r}|}\vec{dr} + V_{xc}[\rho(\vec{r})] \tag{17}$$

The functional of the wavefunction (the total energy of the system) can be calculated from:

$$E[\rho] = \int\psi^*\hat{H}\psi\ \vec{dr} = T + e^2\int\frac{\rho(\vec{r})\rho(\vec{r'})}{|\vec{r}-\vec{r'}|}\vec{dr}\vec{dr}' - e^2\sum_\alpha\frac{Z_\alpha\rho(\vec{r})}{|\vec{R_\alpha}-\vec{r}|}\vec{dr} + E_{xc}[\rho(\vec{r})] \tag{18}$$

The second term represents the repulsive Coulomb energy between the electrons and the third attractive Coulomb energy between the electrons and the ion cores [15].

It is important to realize that the external potential actually defines Hamiltonian since other members are trivially dependent only on the number of electrons in the system. Thus, kinetic energy is generally calculated as the sum of all kinetic energies of efficient electrons [16]:

$$T = \int\psi^*\hat{T}\psi\ \vec{dr} = -\frac{\hbar^2}{2m}\sum_i n_i\int\psi_i^*(\vec{r})\nabla^2\psi_i(\vec{r})\vec{dr} \tag{19}$$

The last term, as known as the exchange-correlation energy, describes all correlation contribution to the total energy. The exchange energy reduces the total energy due to minimalization of the overlap of spatial wavefunctions with the same spin as discussed in the Hartree-Fock approximation section [15].

The correlation energy includes dynamical correlations for electrons with anti-parallel spins because the true wavefunction is not a product of two orbitals as Hartree-Fock approximation assumes, but is rather a complicated function of both variables simultaneously. Only the true wavefunction satisfies the exact Schrödinger equation [17].

These equations are consistently called Kohn-Sham equations leading to Kohn-Sham orbitals (wavefunctions) with Kohn-Sham eigenvalues [15].

### 2.2.7 Exchange-correlation energy

The derived equations are accurate in the sense that no approximation was made during derivation. Expressions for the kinetic energy and the Coulomb potential energy are known but there are no precise expressions for the exchange-correlation energy.

Because the exact expression is not known, several different families of functionals, which try to estimate this potential, was formulated. They differ in their degree of accuracy, computational demands and their focus. The two basics are the local density approximation (LDA) and the generalized gradient approximation [15].

#### Local Density Approximation

The LDA is based on the idea of the homogeneous electron gas. It rests on two assumptions – exchange and correlation energy are dominated by the density in the immediate vicinity of a point $r$ and electron density do not vary strongly with a position. Thus, the LDA works well for $s$, $p$, $4d$ and $5d$ metals but fails in systems with strongly varying electron densities (*e. g.* $3d$ metals).

The exchange-correlation energy of local density approximation:

$$E_{xc}^{LDA} = \int \rho(\vec{r})\epsilon(\vec{r})_{xc}\ \vec{dr} \tag{20}$$

where $\epsilon(\vec{r})$ is the exchange-correlation energy of the density $\rho$ relative to one electron which consists of exchange energy and correlation energy [15].

For the exchange energy exists analytic function based on the Slater determinant and the correlation energy is calculated by accurate Monte Carlo calculations, combined with known exact limiting values [16, 17].

The exchange energy of the system is typically underestimated by about 10 %. Contrary the correlation energy of the system is overestimated 2 or 3 times, but because exchange is about a factor of 10 bigger than correlation, the net exchange-correlation energy is typically underestimated by about 7 % [17].

Although for a large number of systems LDA produces relatively accurate energy, thanks to lower exchange-correlation energy it often overtakes binding energy resulting in an underestimation of equilibrium volume in comparison with the experiment volume [15, 16].

#### Generalized Gradient Approximations

The LDA works well on systems where the electron density does not change much. For systems where electron density is highly variable, it fails and therefore has been formulated Generalized

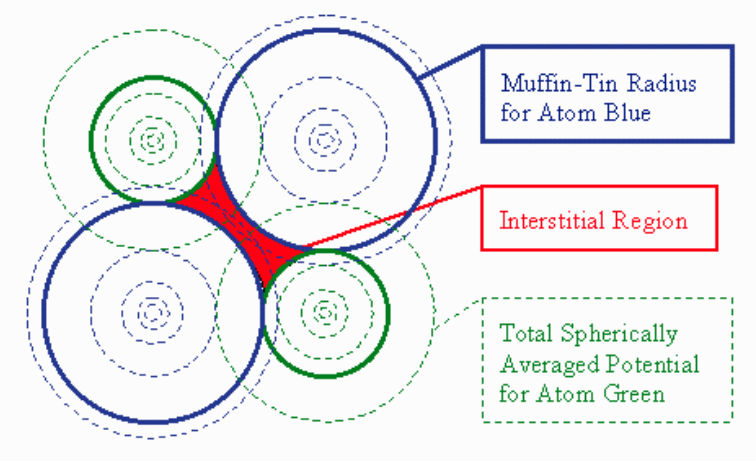


Figure 2: Construction of the Muffin-Tin Potential [19].

Gradient Approximations (GGA) which depends not only on the local electron density but also on the density gradients at the given point [15]:

$$E_{xc}^{GGA} = \int f[\rho(\vec{r}), \nabla\rho] \; \vec{dr} \tag{21}$$

The effect of gradients decreases correlation relative to exchange. This is because in regions of the high gradient the exchange effect keeps electrons apart so that their correlation energy becomes relatively smaller [17].

This exchange-correlation approximation improves total energies, energy barriers, and structural energy differences for systems where electron density is highly variable.

It also expands and softens bonds, but on the other side often overcorrects the local density approximation results [15].

### 2.2.8 Choice of basic functions

There are a large number of DFT implementations that differ primarily in the choice of basic functions. Nowadays the augmented plane wave method (APW) prevails. This method was introduced by Slater in 1937 [18]. The basic idea is the partitioning of space into contiguous spheres surrounding each atom, and an interstitial region between these spheres as shown in Fig. 2. This enables the potential to be spherically-averaged with respect to each atomic center in each sphere and volume-averaged with respect to the interstitial region.

Then the Kohm-Sham equations within spheres are obtained by transforming into spherical coordinates and separating the radial and angular variables. The wavefunctions are then given as a product of a radial function $R_{nl}(\vec{r})$ and spherical harmonic function $Y_{lm}(\theta, \phi)$:

$$\psi(\vec{r}) = R_{nl}(\vec{r}) Y_{lm}(\theta, \phi) \tag{22}$$

Since the potential in the interstitial region is chosen as a constant, the solution for the Kohm-Sham solutions in the interstitial region are plane waves:

$$\psi(\vec{r}) = e^{i\vec{k}\cdot\vec{r}} \tag{23}$$

Thus, with defined bases, it is possible to express any result in the corresponding superposition of the basis function.

The computational disadvantage of this method is that basis functions, through radial solutions, depend on energy. This problem was solved by Andersen who suggested that this problem could be linearized by associating two radial wavefunctions per angular momentum number at each energy: the solution of the radial equation and its energy derivative. As a result, the nonlinear dependence of the wavefunction on energy is neglected. Andersen's linearization is known as full-potential linear augmented plane-wave (FLAPW) method.

Core electrons do not play a role in many physical properties. Thus, core electrons and nuclei can be replaced by a "pseudopotential" and only outer electrons are calculated.

But there are differences between the real potential and the pseudopotential. The real potential is singular near the ion core, but the pseudopotential is finite near the position of a nucleus and thus much smoother. This allows the pseudopotential to expand into plane waves, what is considerably conceptual and computationally simplified.

The main advantage of pseudopotential is that core electrons are pre-calculated in an atomic environment and kept frozen in the course of the other calculations. So instead of being calculated every time, they are calculated only once, saving a lot of computing time.

Methods using pseudopotential are called projector augmented wave (PAW) method [15].

### 2.2.9 Hubbard $U$ correlation

Although DFT provides very accurate results for many systems it fails in calculations of electron structure with partly filled valence d or f shells. This failure of DFT is often described on the example of Mott insulators where the DFT predicts metallic ground states instead of experimentally observed insulating ones [20].

The precise description of Mott insulator requires the full account of the multi-determinant nature of the N-electron wavefunction and of the many-body terms of the electronic interactions because the insulating character of the ground states comes from the strong Coulomb repulsion between electrons which forces them to be localized atomic-like orbitals [21].

Due to the strongly localized motion, they become "correlated" and their wavefunction acquire a many-body character. Thus, the Hartree-Fock method which variationally optimizes single determinant in order to the accurate description of the electronic ground state is not able to capture the physics of Mott insulators [21].

The DFT would describe the behavior of these systems correct if exact exchange-correlation energy functional was known. But DFT predicts metal behavior instead of insulator behavior

because most approximate exchange-correlation potential have a tendency to overdelocalize valence electrons and to overstabilize metallic ground states due to the imprecise account of the exchange interaction and the consequent incomplete cancellation of the electronic self-interaction error.

Hubbard model is one of the simplest model that is able to improve the DFT results in the physics of correlated materials. This real-space second-quantization formalism is perfectly suitable for the description of systems with electrons localized on atomic orbitals. In its simplest, one-band incarnation, the Hubbard Hamiltonian can be written as:

$$H_{Hub} = t \sum_{<i,j>,\sigma} (c^{\dagger}_{i,\sigma} c_{j,\sigma} + h.c.) + U \sum_{i} n_{i,\uparrow} n_{i,\downarrow} \tag{24}$$

where $< i, j >$ detonates the nearest-neighbor atomic sites, $c^{\dagger}_{i,\sigma} c_{j,\sigma}$ are electronic creation, annihilation and $n_{i,\sigma}$ number operators for electrons of spin $\sigma$ on site $i$.

The first term of Eq. 24 describes the motion of strongly localized electrons by "hopping" process from one atomic site to its neighbors whose amplitude $t$ corresponds to the dispersion (the bandwidth) of the valence electronic states and represents the single-particle term of the total energy.

Due to strong localization, the Coulomb repulsion is only accounted for electrons on the same atom through a term proportional to the product of the occupation numbers of atomic states on the same site. Their strength is called Hubbard $U$ [21].

To the exact description of Mott insulators, the hopping amplitude $t$, and the on-site Coulomb repulsion $U$ are necessary set of parameters because their balance controls the behavior of these systems and the character of their electronic ground state.

Generally, the insulating character of the ground state emerges when the energy minimized by electronic delocalization on more extended states is overcomed by short-range Coulomb interactions (the energy cost of double occupancy of the same site). In this case $t << U$. Thus, electrons cannot hop around because of lack of sufficient energy to overcome the repulsion from other electrons on neighboring sites.

Implementation of Hubbard model to DFT is simple and consists in using the Hubbard Hamiltonian for the description of "strongly correlated" electronic states (primarily localized $d$ or $f$ orbitals), while the rest of valence electrons are treated with "standard" approach. The total energy of a system can then be written as:

$$E_{DFT+U}[\rho(\vec{r})] = E_{DFT}[\rho(\vec{r})] + E_{Hub}[\{n^{I\sigma}_{mm'}\}] - E_{dc}[\{n^{I\sigma}\}] \tag{25}$$

where $E_{dc}$ represents so-called "double-counting" (dc) term whose function is to eliminate from the DFT energy functional the part of the interaction energy already contained in $E_{Hub}$ to avoid double-counting problems.

The correction size to approximate DFT total energy functionals is controlled by the effective on-site electronic interaction (Hubbard $U$) that is not previously known because the value depends not only on elements but also its position in a crystal lattice, the structural and magnetic properties of crystal etc. Therefore, in practical use, this parameter is determined semiempirically based on a search for matching with some experimental properties to predict other system properties [21].

## 2.3 Crystalline solids

Most condensed systems form crystalline solids at the certain conditions. A perfect crystal consists of a space-filling array of periodically repeated identical copies of a single structural unit containing some distribution of mass and charge, called the unit cell. The unit cell can be formed from 1 or more atoms of different kinds. The primitive cell is called the unit cell with the smallest volume $v_0$ enclosed by the three primitive lattice vectors $a_i$ in three dimension space:

$$v_0 = \vec{a}_1 \cdot (\vec{a}_2 \times \vec{a}_3) \tag{26}$$

In the case that a unit cell contains more than 1 atom, the positions of the atoms relative to the center of the cell are called the bases.

A Bravais lattice is an infinite array of equivalent points in d-dimensional space generated by a set of discrete translation operations described by an integral linear combination of independent primitive translations vectors $\vec{a}_i$:

$$\vec{R}_l = l_1\vec{a}_1 + l_2\vec{a}_2 + \cdots + l_d\vec{a}_d \tag{27}$$

where $l$ indexes a particular unit cell with component $l_i$ which are always an integer.

For each position vector $\vec{R}_l$, lattice looks exactly the same, therefore it can be defined translative vector which connects equivalent points in the lattice:

$$\vec{T} = \vec{R}_l - \vec{R}_{l'} \tag{28}$$

All translative vectors have a magnitude equal to or greater than the shortest length vector of the primitive unit cell. Because of multiple choice of a primitive vector are available, set of primitive translation vectors for a lattice is not unique.

Between the most frequently used unit cells belong Wigner-Seitz unit, which can be obtained by constructing perpendicular bisectors to all lattice vectors emerging from a given lattice point. The smallest volume enclosed by planes in this way defines the Widger-Seitz cell [22].

To describe the behavior of electrons in a crystal, a reciprocal lattice is used. The reciprocal lattice is constructed as the inverse space of the real lattice. The reciprocal primitive lattice vectors:

$$\vec{b}_1 = \frac{2\pi(\vec{a}_2 \times \vec{a}_3)}{\vec{a}_1 \cdot (\vec{a}_2 \times \vec{a}_3)} \quad \vec{b}_2 = \frac{2\pi(\vec{a}_3 \times \vec{a}_1)}{\vec{a}_2 \cdot (\vec{a}_3 \times \vec{a}_1)} \quad \vec{b}_3 = \frac{2\pi(\vec{a}_1 \times \vec{a}_2)}{\vec{a}_3 \cdot (\vec{a}_1 \times \vec{a}_2)} \tag{29}$$

with the obvious consequence:

$$\vec{a}_i \cdot \vec{b}_i = 2\pi\delta_{ij} \tag{30}$$

The cell volume in the reciprocal space is defined in the same way as primitive cell (Eq. 31):

$$\vec{b}_1 \cdot (\vec{b}_2 \times \vec{b}_3) = \frac{(2\pi)^3}{|\vec{a}_1 \cdot (\vec{a}_2 \times \vec{a}_3)|} = \frac{(2\pi)^3}{v_0} \tag{31}$$

The analogy of the Bravais lattice vectors (Eq. 27) that connect all equivalent positions in the reciprocal space in three dimensions is defined as:

$$\vec{G}_m = m_1\vec{b}_1 + m_2\vec{b}_2 + m_3\vec{b}_3 \tag{32}$$

The dot product of any $\vec{R}$ vector with any $\vec{G}$ vector results:

$$\vec{R}\cdot\vec{G} = 2\pi l \tag{33}$$

where $l$ is always an integer.

The relation between Bravais lattice vectors in real space Eq. 27 and reciprocal space Eq. 32 also gives:

$$e^{i\vec{G}\cdot\vec{R}} = 1 \tag{34}$$

Then any function with the periodicity of the Bravais lattice can be written as:

$$f(\vec{r}) = \sum_G e^{i\vec{G}\cdot\vec{r}} f(\vec{G}) \tag{35}$$

with $f(\vec{G})$ the Fourier Transform (FT) components.

This leads to the definition of a very important theorem in calculating the electron structure called Bloch's theorem which claims:

*The potential of a single-particle Hamiltonian has a translational periodicity of the Bravais lattice:*

$$V^{sp}(\vec{r}+\vec{R}) = V^{sp}(\vec{r}) \tag{36}$$

The single-particle wavefunction acquires the same values in an equivalent position in the lattice, up to a phase factor:

$$\psi_k(\vec{r}+\vec{R}) = e^{i\vec{k}\cdot\vec{R}}\psi_k(\vec{r}) \tag{37}$$

A primitive cell of Widger-Seitz cell type in a reciprocal space is called the first Brillouin Zone, and all points in this volume can be non-equivalent. If the single-particle solution is found in the first Brillouin Zone, solution for the whole crystal can be assembled because of crystal periodicity as described in Eq. 37 [23].

## 2.4 Elastic properties

Elastic properties of a polycrystalline or multiphase system are described by macroscopic quantities such as the bulk modulus $B$ and the shear moduli $G$. When it is a single crystal, its elastic properties are described by the elastic constants $c_{ij}$ and then elasticity is often described as the special case of long-wavelength lattice vibrations.

Hook's law, which is valid for small disturbation, describes the relation of the elastic strain $\epsilon_{kl}$ to the stress $\sigma_{ij}$:

$$\sigma_{ij} = \sum_{k,l=1}^{3} c_{ijkl}\epsilon_{kl} \tag{38}$$

where $i, j, k$ and $l$ run from 1 to 3. Thus, the elastic properties of a material are described by a fourth-rank elasticity tensor with 81 elements $c_{ijkl}$. Because of symmetry ($c_{ijkl} = c_{jkli} = c_{klij} = c_{lijk}$), the 81 elements are reduced to 21 elements. They can be arranged in symmetric $6 \times 6$ matrix using the Voigt's contraction scheme listed in Tab. 1.

Hook's law from Eq. 38 can be rewritten as:

$$\sigma_{\alpha} = \sum_{\beta=1}^{6} c_{\alpha\beta}\epsilon_{\beta} \tag{39}$$

where:

$$\sigma_{\alpha} = \sigma_{ij}; \qquad \epsilon_{\beta} = \epsilon_{kl} \quad if \quad \beta = 1, 2, 3; \qquad \epsilon_{\beta} = 2\epsilon_{kl} \quad if \quad \beta = 4, 5, 6 \tag{40}$$

Table 1: Voigt's contraction scheme

| i, j or k, l | 11 | 22 | 33 | 23 or 32 | 13 or 31 | 12 or 21 |
|---|---|---|---|---|---|---|
| $\alpha$ or $\beta$ | 1 | 2 | 3 | 4 | 5 | 6 |

The number of independent parameters describing the elastic properties depends on the crystal symmetry. The most symmetric (cubic) crystal can be described by only three elastic coefficients $c_{11}, c_{12}$ and $c_{44}$ [24].

While Hooke's law is a phenomenological way of description of how a solid reacts to an applied stress, a deeper understanding of the influence of the pressure, temperature etc. on the elastic constants is based on derivatives of thermodynamic functions.

The first law of thermodynamics is:

$$dU = TdS + pdV \tag{41}$$

where $U$ represents internal energy, $T$ represents temperature, $S$ represents entropy, $p$ represents pressure (positive stress $\sigma$ corresponds to a negative pressure) and $V$ represents volume.

After resolving the forces and deformations into Cartesian components:

$$dU = TdS + V_0 \sum_{i=1}^{6} \sigma_i d\epsilon_i \tag{42}$$

To eliminate entropic term, it assumes adiabatic deformation ($dS = 0$), which ensures that no heat flows in or out of the volume $V_0$:

$$\sigma_i = \frac{1}{V_0} \left( \frac{\partial U}{\partial \epsilon_i} \right)_{S,\epsilon} \tag{43}$$

where the subscripts indicate that all strains $\epsilon_j \neq \epsilon_i$ are held constant and prefactor $1/\mathrm{V}_0$ ensures that stress $\sigma_i$ is independent of the size of the specimen.

The components of $c_{\alpha\beta}$ of adiabatic elastic coefficients are defined by:

$$(c_{\alpha\beta})_S = \left( \frac{\partial \sigma_\alpha}{\partial \epsilon_\beta} \right)_{S,\epsilon'} = \frac{1}{V_0} \left( \frac{\partial^2 U}{\partial \epsilon_\alpha \partial \epsilon_\beta} \right)_{S,\epsilon'} \tag{44}$$

where all $\epsilon$, except $\epsilon_\alpha$ and $\epsilon_\beta$, are kept constant.

The expression the Hook's law through thermodynamic variables gives us the opportunity to simply switch to higher order elastic constants.

The energy of the crystal can be expanded in powers of the strains $\epsilon_{ij}$:

$$U = U(\epsilon_i = 0) + V_0 \sum c_i \epsilon_i + \frac{1}{2} V_0 \sum c_{ij} \epsilon_i \epsilon_j + \frac{1}{6} V_0 \sum c_{ijk} \epsilon_i \epsilon_j \epsilon_k + ... \tag{45}$$

where $i, j, k$ run from 1 to 6.

If only the first 3 terms of expansion are considered, third-order elastic coefficients is defined [24]:

$$(c_{ijk})_S = \frac{1}{V_0} \left( \frac{\partial^3 U}{\partial \epsilon_i \partial \epsilon_j \partial \epsilon_k} \right)_{S,\epsilon'} \tag{46}$$

Difference between calculation elastic coefficients from analysis of the total energy of strained material and an approach based on the analysis of changes in calculated stress values resulting from changes in the strain, mostly stems from the fact that energy is a scalar quantity while stress is a rank-II tensor. Calculating the elastic constants from the linear formula, unlike the calculation of the elastic constants from the energy, allows providing precise elastic data under given initial stress or strain, including large strains outside the harmonic regime around the equilibrium structure [25].

From elastic coefficients, macroscopic elastic properties can be calculated. The simplest relations are found in single crystals with cubic symmetry [24].

A bulk modulus, which represents a resistant to compressibility, can be calculated:

$$B = \frac{c_{11} + 2c_{12}}{3} \tag{47}$$

A Young's modulus $E$ is defined as the ratio of uniaxial stress to strain measured along the same axis:

$$E = \frac{\sigma_1}{\epsilon_1} \tag{48}$$

A shear stress $G$ is defined as:

$$G = c_{44} \tag{49}$$

## 2.5 Lattice dynamics

The atoms that form a crystalline lattice vibrate about their equilibrium positions with an amplitude that depends on the temperature.

Because of the symmetry of the crystal, thermal vibrations can be described as collective ionic modes. These modes, called phonons, can be excited and populated as electronic states but they are bosons, so they do not have to obey the Pauli exclusion principle as electrons and their total number is not fixed.

In this chapter phonons and the way how can be used to describe thermal properties of solids, are discussed [23].

### 2.5.1 Lattice dynamics in harmonic approximation

To describe the positions of the atomic nuclei in the lattice, equilibrium positions of the atomic nuclei are introduced as the vector with the index zero $\vec{R_0}$ and the current position of the atomic nuclei can then be described as $\vec{R}$:

$$\vec{R} = \vec{R_0} + \vec{u} \tag{50}$$

where $\vec{u}$ indicates a displacement from the equilibrium position.

For ions, the total Hamiltonian $\nu$ can be written as the sum of the kinetic energy and potential for the V ions. This potential can be broken down as:

$$\nu = \nu_0(\vec{R}_{0,kl,...}) + \nu'(\vec{u}_{kl,...}) \tag{51}$$

where $l$ represents the individual primitive unit cell in crystal and $k$ represents the individual atoms in the cell.

The first term corresponds to the energy of the lattice with the atoms in the equilibrium positions and is constant, so it can be neglected to solve the dynamics of the lattice.

Although the harmonic approximation only determines the quadratic expansion in displacement $\vec{u}_{kl}$, it is absolutely sufficient for the precise description of the phonons at temperatures well below the melting point. One particular ion contributes to the whole the total energy of its kinetic energy and its quadratic (harmonic) energy as follows:

$$H'(\vec{u}_{kl}) = \frac{1}{2} M_k \left( \frac{d\vec{u}_{kl}}{dt} \right)^2 + \frac{1}{2} \sum_{k',l'} \phi(kl, k'l') \; \vec{u}_{kl} \; \vec{u}_{k'l'} \tag{52}$$

The first term is the kinetic energy, where $M_k$ is the mass of the atom. The second term determines the energy change caused by the displacement of the ions with the indices $(kl)$ while the other atoms are left in place [26].

The second-order force constants are given by the derivation of the potential of the cores [26]:

$$\phi(kl, k'l') = \frac{\partial^2 \nu}{\partial u_{kl} \partial u_{k'l'}} \tag{53}$$

or can be derived from force $\vec{F}_{kl} = -\frac{\partial \nu}{\partial u_{k'l'}}$ [27]:

$$\phi(kl, k'l') = -\frac{\partial F_{k'l'}}{\partial u_{kl}} \tag{54}$$

Some properties of force constants directly derive from the definition:

1. they are real: $\phi(kl, k'l') = \phi^*(kl, k'l')$
2. they are symmetric: $\phi(kl, k'l') = \phi(k'l', kl)$
3. they depend on indices only over the distance of primitive cells: $|\vec{R}_l - \vec{R}'_l|$
4. the total sum of force constants is zero: $\sum_{k'l'} \phi(kl, k'l') = 0$

Force constants include both direct repulsive Coulomb interaction cores and indirect interactions mediated by electrons. Movement of nucleus leads to a change in the distribution of electron density, which gives rise to forces acting on the surrounding ions.

From the translational symmetry of the force constants $\phi(kl, k'l')$ it follows that the wavefunction of Eq. 52 are plane waves. The displacement of the $k$ ion in the $l$ primitive cell can be related to the displacement of the corresponding ion in the primitive cell at the origin of the coordinate system ($l = 0$) according to:

$$\vec{u}_{kl}(\vec{q}, \sigma) = \vec{u}_{k0} e^{i(\vec{q} \cdot \vec{R}_l - \omega t)} \tag{55}$$

where $\vec{q}$ represents the wavevector and $\omega$ represents the frequency of propagating wave.

Due to the regular distribution of ions in the crystal, it is sufficient to select a wavevector only from the first Brillouin zone to describe all vibration modes.

Substitution Eq. 55 to Eq. 52 gives an equation of motion for one selected atom or it can also be solved through Newton's laws of motion ($ma = F$) for $k$ iont in zero primitive cell:

$$M_k \ \omega^2 \ \vec{u}_{k0} = \sum_{k'l'} \phi(k0, k'l') \ e^{-\vec{q} \cdot \vec{R}_{l'}} \ \vec{u}_{k'0} \tag{56}$$

Now a 3D Fourier transform of force constants with weight modification defines dynamic matrix $D_{kk'}(\vec{q})$:

$$D_{kk'}(\vec{q}) = \sum_{l'} \frac{\phi(k0, k'l') \ e^{-i\vec{q} \cdot \vec{R}_{l'}}}{\sqrt{M_k M_k}} \tag{57}$$

Force constants are a function of position vectors of all lattice atoms, while the dynamic matrix $D_{kk'}(\vec{q})$ is a function of the wavevector of the planar deformation wave propagating in

the crystal. By this transition to frequencies ($\omega$), the equation is simplified to:

$$\sum_{k'=1}^{3s} [D_{kk'}(\vec{q}) - \omega^2 \delta_{kk'}] \vec{u}_{k'0} = 0 \tag{58}$$

where $s$ is number of atoms in the primitive cell.

The non-zero solution of this system of equations is conditioned by the zero of the determinant of this system. Therefore, the condition for the value of $\omega$ is overwritten as follows:

$$det|D_{kk'}(\vec{q}) - \omega^2 \delta_{kk'}| = 0 \tag{59}$$

The general solution that is obtained is called the dispersion relation, i.e. the frequency $w$ dependence on the wave vector $\vec{q}$. From the dispersion relation, three important velocities are determined:

- Long wave limit (sound speed in substance):

$$v_f = \lim_{q \to 0^+} \frac{\omega}{q} \tag{60}$$

- Phase velocity (wave propagation velocity):

$$v_f = \frac{\omega}{q} \tag{61}$$

- Group velocity (energy flow rate):

$$v_f = \frac{d\omega}{dq} \tag{62}$$

### 2.5.2 Energy of lattice vibrations

The energy of the phonon mod can be calculated as:

$$E_n = \hbar\omega \left( \frac{1}{2} + n \right) \tag{63}$$

where $\frac{1}{2}\hbar\omega$ is the zero-point energy of a quantum harmonic oscillator and the quantum number $n$ indicates the number of phonons with the frequency $\omega$ which is at a given temperature given by the Bose-Einstein distribution function [26]:

$$n = \frac{1}{e^{(\hbar\omega)/(k_B T)} - 1}, \tag{64}$$

and therefore energy $E$ of phonon system can be calculated once phonon frequencies over Brillouin zone are known from the canonical distribution in statistical mechanics for phonons under

the harmonic approximation:

$$E = \sum_{\vec{q}m} \hbar\omega(\vec{q}m) \left[\frac{1}{2} + \frac{1}{e^{(\hbar\omega)/(k_B T)} - 1}\right] \tag{65}$$

where $m$ is the band index [27].

### 2.5.3 Mean-square displacement

If vibrational energy is known, the mean-square displacement can be easily calculated. In a harmonic approximation (analogy to a harmonic oscillator), the maximum of kinetic energy equals the maximum of potential energy. For the whole volume $V$ crystal of density $\rho$, the following relationship is obtained by comparing the relations for classical and quantum energy calculations:

$$\frac{1}{2}\left(\frac{1}{2}\rho V\omega^2 u_0^2\right) = \frac{1}{2}\left[\left(n + \frac{1}{2}\right)\hbar\omega\right] \tag{66}$$

The mean square atomic displacement is obtained as [26]:

$$< u_0^2 >= \frac{2(n + \frac{1}{2})\hbar}{\rho V\omega} \tag{67}$$

### 2.5.4 Thermodynamics properties at constant volume

Knowing the lattice dynamics gives opportunities to determine many of temperature-dependent properties of solids. From knowledge of the quantum mechanical energy eigenvalues of these vibrations, easily model thermodynamic quantities as constant volume heat capacity $C_V$, Helmholtz free energy $F_{ph}$ of phonons and entropy $S$ can be computed as functions of temperature [27]:

$$C_V = \left(\frac{\partial E}{\partial T}\right) = \sum_{\vec{q}m} C_{\vec{q}m} = \sum_{\vec{q}m} k_B \left(\frac{\hbar\omega_{\vec{q}m}}{k_B T}\right)^2 \frac{e^{(\hbar\omega_{\vec{q}m})/(k_B T)}}{[e^{(\hbar\omega_{\vec{q}m})/(k_B T)} - 1]^2} \tag{68}$$

$$F_{ph} = \frac{1}{2}\sum_{\vec{q}m} \hbar\omega_{\vec{q}m} + k_B T \sum_{\vec{q}m} ln\left[1 - e^{-(\hbar\omega_{\vec{q}m})/(k_B T)}\right] \tag{69}$$

$$S = -\frac{\partial F}{\partial T} = \frac{1}{2T}\sum_{\vec{q}m} \hbar\omega_{\vec{q}m} coth\frac{\hbar\omega_{\vec{q}m}}{2k_B T} - k_B \sum_{\vec{q}m} ln\left[2sinh\frac{\hbar\omega_{\vec{q}m}}{2k_B T}\right] \tag{70}$$

### 2.5.5 Volume dependence of phonon properties

Phonon properties vary with changes of volume because the crystal potential is an anharmonic function of volume. However, it is possible to calculate the thermodynamic properties in an agreement with experiments from harmonic potential if the temperature is well below the melting point. If volume dependence of phonon properties is calculated so that the harmonic ap-

proximation at each volume is simply applied, it means that the thermodynamic properties are calculated in the so-called quasi-harmonic approximation (QHA).

Volume dependence of thermodynamic variables is more desirable than thermodynamic variables at constant volume since they are more easily measurable in experiments.

The basic problem that needs to be solved is the temperature dependence of equilibrium volume on temperature. This can be achieved by minimizing Gibbs energy at given temperature and pressure:

$$G(T,p) = min_V[F(T,V) + pV] \tag{71}$$

where the minimum value in the square bracket is found by changing volume $V$. Helmholtz free energy $F(T,V)$ consists of internal energy $U(V)$ which is obtained as the total energy of electronic structure from the first principles calculation and $F_{ph}(T,V)$ from Eq. 69.

For each temperature and pressure, the minimum is found, and all the minima then form the volume dependence on temperature. Then properties as volumetric thermal expansion coefficient $\beta$ and heat capacity at constant pressure $C_p$ are obtained from the calculated equilibrium volumes $V(T)$ at dense temperature points $T$:

$$\beta(T) = \frac{1}{V(T)}\frac{\partial V(T)}{\partial T} \tag{72}$$

$$C_p(T,p) = -T\frac{\partial^2 G(T,p)}{\partial T^2} = C_V(T,V(T,p)) + T\frac{\partial V(T,p)}{\partial T}\left.\frac{\partial S(T,V)}{\partial V}\right|_{V=V(T,p)} \tag{73}$$

where the second term of the second equation in Eq. 73 is the contribution to heat capacity from thermal expansion [27].

### 2.5.6 Electron heat capacity

From classical statistical mechanics, it follows that the free particle should have a specific capacity equal $\frac{3}{2}k_B$, where $k_B$ is the Boltzmann constant. If N atoms with one valence electron contribute to electron gas, and if these electrons are freely movable, the contribution to specific heat should be $\frac{3}{2}k_BN$. However, the experimental electron contribution at room temperature is usually 1000 times smaller.

Classical statistical mechanics fails because it does not respect the Pauli exclusion principle which is represented by the Fermi-Dirac distribution function:

$$f(E) = \frac{1}{e^{(E-\mu)/(k_BT)} + 1} \tag{74}$$

where $\mu$ represents chemical potential, which at zero temperature is equal the Fermi energy and at all other temperatures equal 1/2 in the Fermi-Dirac distribution function [28]. The Fermi energy is defined as the value of the energy below which all single-particle states are occupied at 0 K [23].

Upon heating from absolute zero, all electrons do not obtain the $k_BT$ energy as predicted by the classical statistical mechanics, but only the electrons around the Fermi energy are thermally excited. Only these electrons acquire energy in the order of $k_BT$.

The derivation of the heat capacity of the electrons for low temperatures ($k_B << E_F$) can be derived from an increase in the total energy of the electron when heated from absolute zero to T:

$$U(E) = \int_0^\infty E\ D(E)\ f(E)\ dE - \int_0^{E_F} E\ D(E)\ dE \tag{75}$$

where $D(E)$ is the density of state and $f(E)$ is the Fermi-Dirac distribution function.

The number of particles may be written as:

$$N(E) = \int_0^\infty D(E)\ f(E)\ dE \tag{76}$$

By multiplication of $E_F$ is obtained:

$$E_F N(E) = E_F \int_0^\infty D(E)\ f(E)\ dE \tag{77}$$

Derived equations 75 and 77 by temperature lead to:

$$\frac{\partial U}{\partial T} = \int_0^\infty E\ D(E)\ \frac{\partial f(E)}{\partial T} \tag{78}$$

$$0 = E_F \frac{\partial N}{\partial T} = \int_0^\infty E\ D(E)\ \frac{\partial f(E)}{\partial T} \tag{79}$$

Those equations 78 and 79 define the specific heat of electrons in the form:

$$C_{el} = \int_0^\infty (E - E_F)\ D(E)\ \frac{\partial f(E)}{\partial T}\ dE \tag{80}$$

At low temperatures $k_BT/E_F < 0.01$, the partial derivative is large only for energy near $E_F$ and therefore $D(E)$ can be put before the integral:

$$C_{el} = D(E) \int_0^\infty (E - E_F)\ \frac{\partial f(E)}{\partial T}\ dE \tag{81}$$

For low temperatures, chemical potential $\mu$ can also be replaced by constant Fermi energy $E_F$ because $E_F$=$\mu(0)$. Then:

$$\frac{\partial f(E)}{\partial T} = \frac{E - E_F}{k_B T^2} \frac{e^{(E-\mu)/(k_BT)}}{[e^{(E-\mu)/(k_BT)} + 1]^2} \tag{82}$$

Thus, the electronic heat capacity is [28]:

$$C_{el} = \frac{1}{3}\pi^2 D(E_F) k_B^2 T \tag{83}$$

This expression is qualitatively correct for simple, free-electron like metals and alloys where narrow energy interval around the Fermi energy is assumed and therefore the density of states can be regarded as a constant and equal to $D(E_F)$.

However, an electron-phonon many-body enhancement factor, which stems from interaction of electrons with phonons, is always present. Its value is approximated empirically by $1 + \lambda_{el-ph}$ with typical value for metals of 1.4 but occasionally (e.g. Pb, Hg) can be as large as 2.5.

The electron-phonon many-body enhancement factor is temperature dependent and disappears at high temperatures [24].

# 3 Methodology

All of the DFT calculations in this thesis were carried out using the Vienna Ab Initio Simulation Package (VASP) [29] with the projector augmented wave scheme (PAW). Electron exchange and correlation potentials were treated within the generalized gradient approximation of Perdew-Burke-Ernzerhof (PBE) [30] as well as with its revised version, so-called (PBEsol) [31].

The semi-core and valence electrons are in the $6s^2\,6p^6\,6d^2\,7s^2\,5f^0$ configuration for thorium, $6s^2\,6p^6\,6d^2\,7s^2\,5f^1$ configuration for protactinium and $2s^2\,2p^2$ configuration for carbon.

The kinetic energy cut-off for the plane-wave basis functions is 500 eV. Brillouin zone integrations were carried out using 16 x 16 x 16 Γ-centered k-point mesh for thorium and 12 x 12 x 12 Γ-centered k-point mesh for actinide monocarbides. The 4 x 4 x 4 supercells containing 64 atoms with the 6 x 6 x 6 Γ-centered k-point mesh for thorium and the 2 x 2 x 2 supercells containing 64 atoms with the 4 x 4 x 4 Γ-centered k-point mesh for actinide monocarbides were used to calculate the vibrational properties using the direct force-constant method as implemented in the PHONOPY [27] code.

The spin-orbit interaction (SOI) is included and the Hubbard $U$ correction [20] is applied to actinide 5*f*-states. The components of the elastic tensor are calculated from the strain-stress relationship [25]. The Sommerfeld coefficients are calculated from Eq. 83.

The convergence criteria for the system total energy and residual Hellmann-Feynman forces are set to $10^{-7}$ eV and $10^{-6}$ eV/Å, respectively. Bulk moduli were obtained from fits to Vinet's equation of state [32].

# 4 Results and Discussion

## 4.1 Thorium

A lot of theoretical works on thorium have been done [33-39] with different approaches but none of them can reproduce all elastic constants, especially problematic is $c_{12}$. Of all the theoretical work, only a few authors [33, 34] take into account the spin-orbit interactions and all the theoretical DFT works treat 5*f*-states without localization correction. However, the recent DFT study [40] that addressed the structural, electronic, magnetic, elastic properties and lattice dynamics has shown that it is necessary to detonate the effective on-site Coulomb repulsion interaction parameter between the 5*f*-states and take into account the spin-orbit interactions for realistic theoretical description of the ground-state properties of uranium carbide.

In this work, it is investigated whether is including spin-orbit interaction and varying on-site Coulomb interactions can improve agreement between theoretical and experimental results and therefore is needed for the correct electronic structure and lattice dynamics description of actinides within density functional theory.

### 4.1.1 Electronic structure

Precise determination of the electronic structure is crucial for accurate and a realistic description of the lattice dynamics. Therefore, the effect of SOI and the effect of Hubbard $U$ parameter on the electronic structure of thorium is thoroughly analyzed.

First, a modification of the electronic structure upon SOI with treating the 5*f*-states as fully delocalized ($U_{eff} = 0$ eV) is presented.

Figure 3 shows modification caused by the inclusion of SOI, *i.e.* splitting into well separated $6p_{1/2}$ and $6p_{3/2}$ subbands by about 5 eV and splitting into well separated $5f_{5/2}$ and $5f_{7/2}$ subbands which amounts to 2 eV. However, states around the Fermi energy ($E_F$) are not significantly affected by the inclusion of SOI. The conduction bands consist essentially of $5f$-states with a minor presence of 6*d*-states.

Next, in Fig. 3 is presented evolution of total densities of electronic states as a function of the Hubbard $U$ which varies the localization of the 5*f*-states. It is observed a similar behavior to that of spin-orbital interaction, there is no significant change in total electronic density in vicinity of the Fermi energy ($E_F$). Thorium has very few 5*f*-states (ca. 0.4 electron) under the Fermi level ($E_F$) and changes of 5*f*-states due to Hubbard $U$ modification begin to show up from $E = 1.2$ eV above $E_F$ which would correspond to 1 occupied $5f$ electron. However, the localization of $5f$ electrons results in shifts of $6s$, $7s$ and $6p$-states to lower energies.

Lattice parameters and Sommerfeld coefficient as function of inclusion of SOI and Hubbard parameter $U$ correction in the range 0-2 eV are shown in the Table 2. Lattice parameter gets smaller by around 0.5% as a result of presence of the SOI. In contrast, the increase of 5*f*-states localization increased the lattice parameter as expected.

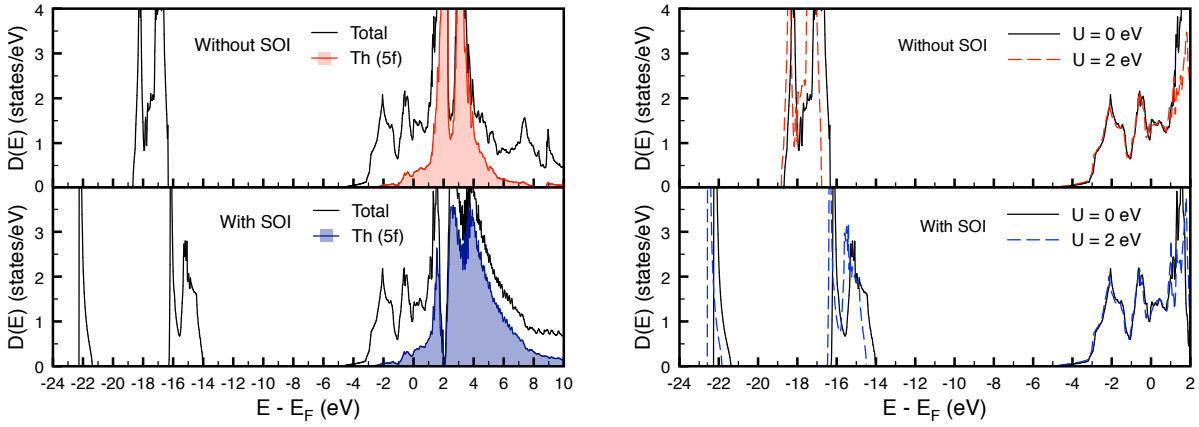


Figure 3: Total and 5f-orbital projected densities of electron states D(E) for $fcc$ thorium with fully itinerant $5f$ electrons ($U_{eff} = 0$ eV) and with SOI neglected and included (left) and as function of Hubbard $U$ parameter with SOI neglected and included (right).

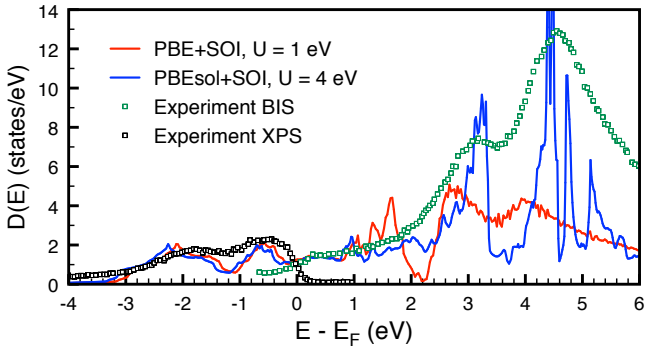


Figure 4: Comparison of the total electron densities of states $D(E)$ of two different exchange and correlation potential with the BIS and XPS measurements [43] in thorium.

Comparison of Sommerfeld coefficients between DFT+SOI, DFT+U or DFT+SOI+U confirms that the electronic density does not change significantly near the Fermi energy $N(E_F)$. Nevertheless, the density of states with the inclusion of SOI gives slightly better results when compared to experimental measurements [41, 42]. Our calculated Sommerfeld coefficients are increased by the electron-phonon many-body enhancement factor equals 1.4, which is typically value [24].

The density of state accuracy can be checked with BIS and XPS measurements [43]. Fig. 4 shows that our result of PBE+SO+U agrees with the XPS experiment but fails with BIS experiment. It is not possible to reproduce BIS experiment and experimental lattice parameter at the same time with PBE. However, the consistency with the XPS and even BIS experiment is found at PBEsol+SOI+U, where the Hubbard $U$ parameter was tuned to the experiment lattice constants as listed in Table 2. The high value of Hubbard $U$ parameter acting on $5f$-states is needed for correct description of states above the Fermi energy $N(E_F)$ and this type of exchange

Table 2: Calculated and experimental lattice parameters ($a$), elastic constants $c_{ij}$, bulk modulus $B$, Sommerfeld coefficient $\gamma$, debye temperatures $\theta_D$ and force constants $\Phi$ for *fcc* thorium

| | $E_{xc}$ | $U$ (eV) | $a$ (Å) | $c_{11}$ (GPa) | $c_{12}$ (GPa) | $c_{44}$ (GPa) | B (GPa) | $\gamma$ (mJ K$^{-2}$ mol$^{-1}$) | $\theta_D$ (K) | $\Phi$ (Nm$^{-1}$) | Rerefence |
|---|---|---|---|---|---|---|---|---|---|---|---|
| VASP | PBE | 0.0 | 5.049 | 81 | 43 | 53 | 55 | 4.59 | 186 | 82 | This work |
| | PBE | 1.0 | 5.092 | 79 | 45 | 48 | 56 | 4.68 | 167 | 78 | This work |
| | PBE | 2.0 | 5.125 | 77 | 47 | 45 | 58 | 4.47 | 153 | 76 | This work |
| | PBE+SOI | 0.0 | 5.023 | 86 | 45 | 56 | 58 | 4.42 | 179 | 88 | This work |
| | PBE+SOI | 1.0 | 5.064 | 83 | 47 | 50 | 59 | 4.16 | 163 | 85 | This work |
| | PBE+SOI | 2.0 | 5.099 | 79 | 50 | 46 | 60 | 3.86 | 153 | 81 | This work |
| | PBEsol+SOI | 4.0 | 5.069 | 80 | 59 | 42 | 67 | 3.50 | 144 | 84 | This work |
| FP-LMTO | | | 4.910 | 55 | 35 | 46 | 63 | | | | Söderlind [33, 34] |
| ABINIT | PBE | 0.0 | 5.024 | 84 | 40 | 58 | 55 | | | | Bouchet [35] |
| WIEN2K | PBE | 0.0 | 5.062 | 76 | 41 | 53 | 57 | | | | Gupta [36] |
| Model pot. | | | | 78 | 62 | 40 | 68 | | | | Baria [37] |
| VASP | PBE | 0.0 | 5.062 | 81 | 41 | 49 | 50 | | | | Hu [38] |
| WIEN2K | PBE | 0.0 | 5.080 | 76 | 44 | 44 | 55 | | | | Jaroszewicz [39] |
| Exp. | | | 5.085 | 81 | 50 | 50 | 60 | | | | Greiner [44] |
| Exp. | | | 5.089 | 78 | 48 | 51 | 58 | | | | Armstrong [45] |
| Exp. | | | | | | | | 4.23 | 167 | | Schmidt [41] |
| Exp. | | | | | | | | 4.31 | 163 | | Gordon [42] |

and correlation potential should be used for calculation of optical properties.

### 4.1.2 Elastic properties

There are three elastic constants, namely $c_{11}$, $c_{12}$ and $c_{44}$, in a cubic crystal structure. The results are presented in Table 2 and compared to the ones obtained with other theoretical and experimental studies for *fcc* Th. All previous theoretical calculations [33, 34, 35, 36, 37, 38, 39] fail to fully reproduce all elastic constants, especially $c_{12}$, which is in most calculations significantly underestimated.

Our results are similar to the others if SOI or Hubbard $U$ correction is not included, *i.e.* $c_{11}$ and $c_{44}$ are in very good agreement with experimental values [44, 45] and $c_{12}$ is largely underestimated. Although the inclusion of SOI increases problematic $c_{12}$, simultaneously also increases $c_{11}$ and $c_{44}$ further from experimental values. It is the SOI and increase of the 5*f*-states localization at the same time that leads to excellent agreement with the experiment since localization of 5*f*-states reduces $c_{11}$ and $c_{44}$ values and simultaneously increases $c_{12}$. The value of $U_{eff} = 1$ eV seems to address correct description of mechanical properties.

Although only PBEsol exchange and correlation potential gives excellent agreement with BIS measurement, it fails to reproduce elastics coefficients and bulk modulus. PBEsol+SOI calculation overestimated $c_{44}$ and underestimate $c_{12}$ from redundant localization of 5*f*-states. It confirms that for mechanical properties it is not important to describe unoccupied states well above the Fermi energy but only occupied states are important.

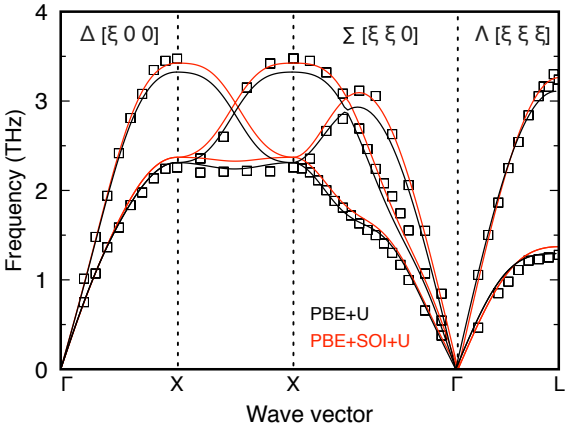


(a) Dispersion relations of *fcc* thorium phonons. White squares are experimental data [46].

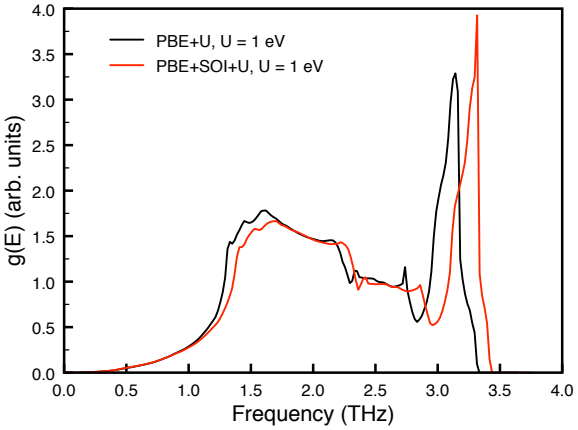


(b) Phonon densities of states G(E) of *fcc* thorium metal.

### 4.1.3 Phonons

For *fcc* structure, there is only one unique atom in its primitive cell, thus there are only three independent phonon modes in the dispersion relations. The phonon dispersion curves of thorium have been carried out along directions $\Delta[\xi\ 0\ 0]$, $\sum[\xi\ \xi\ 0]$ and $\Lambda[\xi\ \xi\ \xi]$ at zero temperature with a comparison of experimental data obtained from neutron-scattering measurement at ambient condition [46] as presented in Fig. 5a. Figure 5a reveals that the shift to higher frequencies from the inclusion of the SOI is needed to correctly describe the dispersion relations of the longitudinal phonon branches. However, the difference between frequencies is based primarily on different lattice constants. DFT+U overestimates experimental lattice parameter and therefore vibrates at lower frequencies than experimentally measured. Lattice parameter reduction is a key factor in which SOI indirectly causes more accurate lattice dynamics.

Both phonon dispersion relations of *fcc* thorium reproduce the anomalous behavior of the transverse branches along $\sum[\xi\ \xi\ 0]$ direction. It means that this anomaly is based purely on phonons and does not arise from the electron-phonon interaction as claimed by authors of Ref. [46].

One of the most important parameters determining the thermal characteristics of materials is the Debye temperature ($\theta_D$) and on-site force constants ($\Phi$), both quantities summarized in Table 2. The inclusion of Hubbard $U$ correction seems to be crucial for the correct description of the Debye temperature of thorium because without correction is $\theta_D$ overestimated around 10 % over experimental measurements [41, 42].

The value of $\theta_D = 167K$ with the choice $U_{eff} = 1$ eV is in agreement with experiments [41, 42]. Whereas inclusion of SOI has an only weak effect on Debye temperature: $\theta_D = 163K$.

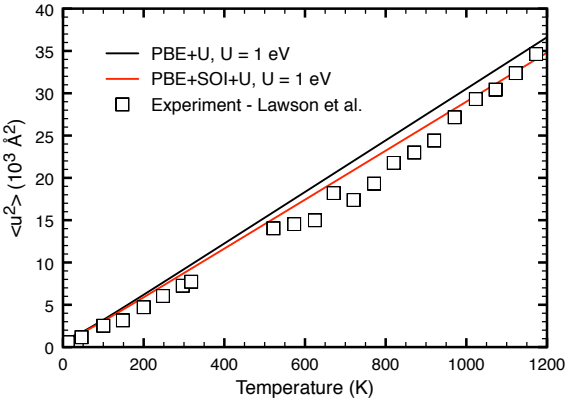


(a) Calculated mean-square thermal atomic displacement versus temperature for *fcc* thorium with comparison of experimental data [47].

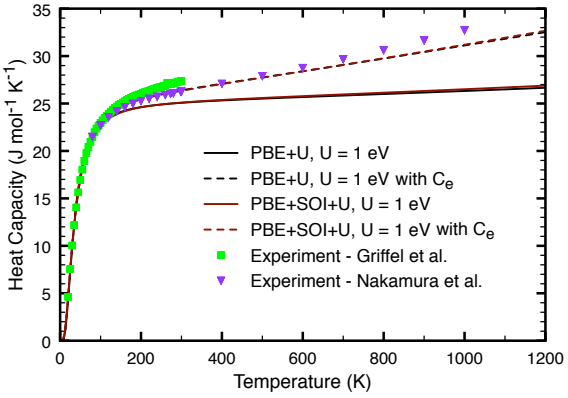


(b) Heat capacity at constant pressure as a functions of temperature in comparison with the experimental values [48, 49].

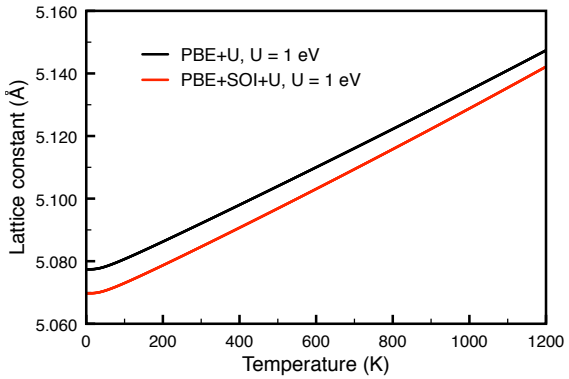


(a) Lattice parameter as a functions of temperature for *fcc* thorium.

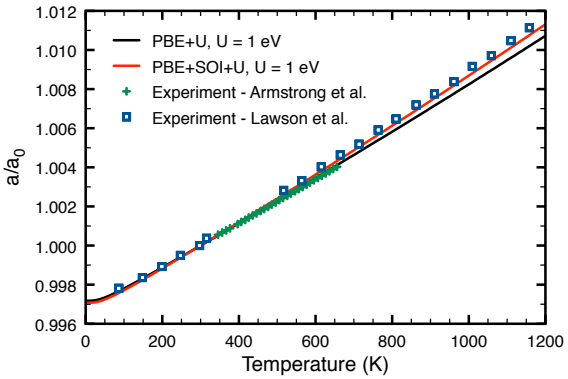


(b) Reduced lattice constants $a(T)/a_0$ versus temperature for *fcc* thorium.

### 4.1.4 Thermodynamic properties

The thermal properties are evalued from the lattice dynamic calculations for the temperature range of 0-1200 K.

Mean square displacements in the direction [1 0 0] are displayed in Fig. 6a. DFT+SOI+U is in good agreement with experimental measurement [47] and DFT+U overestimates mean square displacement due to a larger lattice constant.

The heat capacities at constant pressure with and without the electronic contribution ($C_e$), which are depicted in Fig. 6b, grow very fast at low temperatures and reach the Dulong-Petit limit of 3R valid for heat capacity at constant volume at 187 K. After rapid growth at low temperatures, linear growth stemmed mainly from the electronic contribution. Heat capacity of thorium is not sensitive to spin-orbit effects. The high-order anharmonicity becomes more prominent around 700 K.

Fig. 7a represents thermal expansion of *fcc* thorium. Unfortunately, no temperature dependent experimental data of lattice constants are available. Only existing experimental data

related to thermal expansion of thorium are obtained using $(a - a_0)/a_0$ relation, where $a_0$ is the lattice constant at 297 K. Fig. 7b demonstrates excellent agreement with both experimental measurement [45, 47]. Unlike heat capacity, the inclusion of SOI is needed to accurately describe thermal expansion at higher temperatures.

## 4.2 Thorium and Protactinium monocarbide

After the thorough analysis of thorium metal where excellent agreement with experimental measurements is found, thorium and protactinium monocarbides are analyzed. Detailed analysis of ThC and PaC is important because those monocarbides are assumed as potential nuclear fuels of generation IV nuclear reactors [10].

A lot of properties were experimentally measured on thorium monocarbide. On the contrary, protactinium monocarbide is unexplored and only known experimental data is lattice parameter. The explanation is simple. As mentioned in theoretical part of the thesis, the protactinium is very rare element because of high radioactivity and thus measurement of any protactinium compound is difficult.

However, these difficulties are not the problem of theoretically investigation and protactinium monocarbide can be theoretical analyzed in the same manner as the other compounds. Because of missing experiments, all protactinium monocarbide properties presented in this thesis are a prediction.

Thorium metal and actinide monocarbides differ to each other. Thorium at ambient conditions is pure metal with dominant metallic bonding. Adding carbon significantly changes electron structure as depicted in Fig. 8. A significant part of bonding in light actinide monocarbides forms ionic bonding due to considerable electronegativity difference between actinide and carbon. But actinide monocarbides keep their metallic behavior thus metallic bonding is also presented. Due to well-known hybridization of actinide $6d$, $5f$ and carbon $6p$ orbitals, weak covalent part of bonding is included as well. So, considerable different electronic, mechanical and phonon properties of thorium metal and actinide monocarbide are expected.

As far as magnetism is concerned, thorium monocarbide is paramagnetic and protactinium monocarbide is diamagnetic [50].

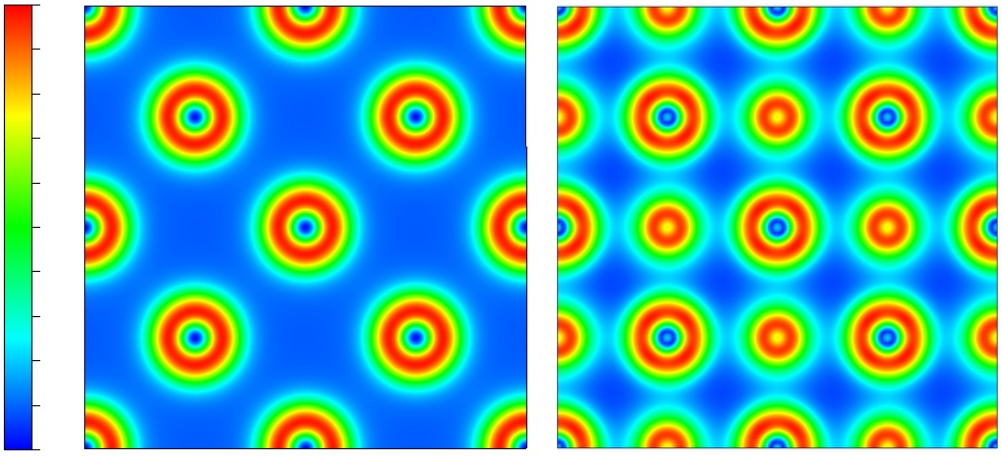

Figure 8: The charge density of valence electrons of thorium metal and thorium monocarbide in the plane (0 0 1). Dark blue represents zero charge density and red maximum intensity.

Theoretical investigation of actinides within DFT is not straightforward due to a strong influence of correlated states and relativistic effects. Many previous theoretical works investigated thorium [51-54] and protactinium monocarbide [58] neglect them. Hence, the spin-orbital interaction and Hubbard $U$ correction is incorporated into our calculations. Comparison of results, which take into account and ignore these effects, is provided.

### 4.2.1 Electronic structure

The first difference between thorium metal and thorium monocarbide is in the value of Hubbard term U needed to a reproduction of experimental lattice parameter. Both values of the Hubbard $U$ parameters have to be reduced by 1 eV with respect to values used in pure metal. So the agreement with experimental measurements is found at $U_{eff} = 0$ eV for PBE+SOI and $U_{eff} = 3$ eV for PBEsol+SOI as listed in Table 3.

It is assumed that carbon atoms with higher electronegativity drain electrons from thorium atoms and Coulomb repulsion on same atomic site represented by Hubbard $U$ term is reduced.

While thorium metal electron densities of states of PBE+SOI and PBEsol+SOI are very similar, not a negligible difference exists in case of both monocarbides as shown in Fig. 9. Especially at the vicinity of the Fermi energy, which consists of hybridized thorium $6d$, $5f$ and carbon $2p$ states, a difference in DOS is found.

#### Thorium monocarbide

From the investigation of *fcc* thorium electronic structure emerges that PBE+SOI ($U_{eff} = 1$ eV) and PBEsol+SOI ($U_{eff} = 4$ eV) are equivalently able to reproduce the ground state electronic states (see XPS experiment in Ref. [43]). Because there are no XPS, UPS or BIS experiments available for thorium or protactinium monocarbides, which would clearly identify the correct way to describe these systems, it is assumed that the same approach used for thorium metal is also suitable for actinide carbides.

Number of states at the Fermi energy, which is directly connected to Sommerfeld coefficient, indicates that more accurate DOS is based on PBEsol+SOI ($U_{eff} = 3$ eV) because its Sommerfeld coefficient value of 2.47 $mJK^{-2}mol^{-1}$ is much closer to experimental values (2.1–2.9 $mJK^{-2}mol^{-1}$ [55, 56]) than 4.29 $mJK^{-2}mol^{-1}$ predicted by PBE+SOI ($U_{eff} = 0$ eV). Calculated values do not include an electron-phonon many-body enhancement factor because thorium monocarbide is not simple metal as thorium and thus the electron-phonon many-body enhancement factor can take both higher as well as lower then 1.4 value.

The amount of occupied $5f$ states is also different. The higher value of Hubbard $U$ parameter for PBEsol+SOI causes a bigger obstacle to delocalization of $5f$ states and therefore occupation of $5f$ states is about one-third less in comparison with PBEsol+SOI ($U_{eff} = 0$ eV).

Semi-core thorium $6s$ and $6p$ located around -21 eV and -15 eV below the Fermi level remain almost unchanged as well as carbon $2s$ states extending from -10 to -7 eV.

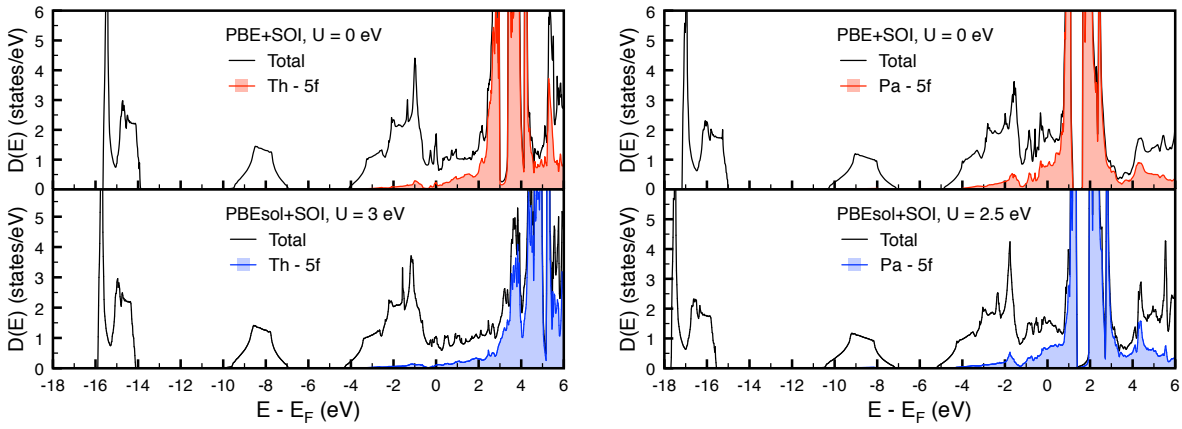


(a) ThC (b) PaC

Figure 9: Total and $5f$-orbital projected densities of electron states D(E) calculated with PBE+SOI and PBEsol+SOI with different Hubbard $U$ parameter.

### Protactinium monocarbide

The lattice parameter of PaC was experimentally measured by Hery et al. and Lorenz et al. [50, 57] and their results are presented in Table 3. The Hubbard $U$ parameter was tuned to match their measurement and results $U_{eff} = 0$ eV for PBE+SOI and $U_{eff} = 2.5$ eV for PBEsol+SOI.

The course of the electronic density of states of protactinium monocarbide is very similar to thorium monocarbide. All electron states are shifted to lower energy due to stronger attractive Coulomb interactions but generally, there is no significant difference from thorium monocarbide as shown in Fig. 9.

Occupation of the $5f$ band in comparison with thorium monocarbide is increased not only because of the energy shift but also because of one more electron in the system. As a result, at the least one $5f$ electron is occupied in protactinium monocarbide as in an isolated protactinium atom unlike in ThC.

The higher value of Hubbard $U$ correlation again causes bigger occupation (around 20 %) of $5f$ states in PBE+SOI ($U_{eff} = 0$ eV) compared with PBEsol+SOI ($U_{eff} = 2.5$ eV).

Experimental Sommerfeld coefficient is unknown and therefore calculated values 4.14 $mJK^{-2}mol^{-1}$ from PBE+SOI ($U_{eff} = 0$ eV) and 3.58 $mJK^{-2}mol^{-1}$ from PBEsol+SOI ($U_{eff} = 2.5$ eV) are predictions. The electron-phonon many-body enhancement factor is not included. The predicted values are much similar to each other than in case of thorium monocarbide.

Only one theoretical work on protactinium monocarbide has been done [58]. The presented electronic density of states in this thesis and in the previous theoretical calculation are perfectly matched.

Table 3: Calculated and experimental lattice parameters ($a$), elastic constants $c_{ij}$, bulk modulus $B$, Sommerfeld coefficient $\gamma$, and Debye temperatures $\theta_D$ for *NaCl-type* ThC and PaC

| | | $E_{xc}$ | $U$ (eV) | $a$ (Å) | $c_{11}$ (GPa) | $c_{12}$ (GPa) | $c_{44}$ (GPa) | B (GPa) | $\gamma$ (mJ K$^{-2}$ mol$^{-1}$) | $\Phi$ (K) | Rerefence |
|---|---|---|---|---|---|---|---|---|---|---|---|
| ThC | VASP | PBE+SOI | 0.0 | 5.339 | 217 | 86 | 78 | 130 | 4.29 | 225 | This work |
| | VASP | PBEsol+SOI | 3.0 | 5.328 | 265 | 85 | 83 | 145 | 2.47 | 249 | This work |
| | WIEN2k | PBE | 0.0 | 5.388 | 252 | 96 | 60 | 148 | 1.71 | | Shein [51] |
| | WIEN2k | PBE+SOI | 0.0 | 5.388 | 163 | 70 | 54 | 100 | 2.59 | | Shein [51] |
| | CASTEP | PBE | 0.0 | 5.341 | 276 | 99 | 87 | 158 | | 458 | Aydin [52] |
| | CASTEP | LDA | 0.0 | 5.269 | 241 | 96 | 78 | 145 | | 478 | Aydin [52] |
| | CASTEP | LDA+U | 2.3 | 5.336 | 215 | 88 | 81 | 130 | | 470 | Aydin [52] |
| | ESPRESSO | PBE | 0.0 | 5.335 | 222 | 86 | 66 | 131 | | 298 | Daroca [53] |
| | VASP | PBE | 0.0 | 5.348 | 216 | 89 | 80 | 137 | | 258 | Sahoo [54] |
| | Exp. | | | 5.335 | | | | | | | Street [63] |
| | Exp. | | | 5.322 | | | | 109 | | | Gerward [59] |
| | Exp. | | | 5.340 | | | | 147 | | | Yu [60] |
| | Exp. | | | | | | | | 2.9 | 280 | Harness [55] |
| | Exp. | | | 5.344 | | | | | 2.1 | 262 | Danan [56] |
| PaC | VASP | PBE+SOI | 0.0 | 5.063 | 305 | 102 | 75 | 170 | 4.14 | 299 | This work |
| | VASP | PBEsol+SOI | 2.5 | 5.059 | 378 | 104 | 86 | 190 | 3.58 | 323 | This work |
| | VASP | PBE | 0.0 | 5.081 | 308 | 108 | 72 | 167 | | 343 | Çiftci [58] |
| | Exp. | | | 5.057 | | | | | | | Hery [50] |
| | Exp. | | | 5.061 | | | | | | | Lorenz [57] |

### 4.2.2 Elastic properties

Bulk modulus is the only elastic property that was measured for thorium monocarbide. However, experimental studies are not consistent. Gerward *et al.* [59] report the bulk modulus of 109 GPa while Yu *et al.* [60] report the bulk modulus of 147 GPa. Olsen *et al.* [61] claim that the discrepancy is possibly due to the difference of stoichiometry. Sample of Yu *et al.* [60] had a composition corresponding to $ThC_{0.95}$ but Gerward *et al.* [59] have much less stoichiometric of $ThC_{0.76}$. The value of 147 GPa is supported by comparison with the lattice parameters and bulk moduli of thorium nitride (ThN) and thorium sulphide (ThS) [60].

The PBEsol+SOI+U potential with calculated value of 145 GPa is in excellent agreement with Yu *et al.* [60] experiment. The PBE+SOI potential with 130 GPa underestimates this result as many other theoretical works [52-54].

Then the predicted value of bulk modulus for protactinium monocarbide is 190 GPa which is 14% more than predicted by Çiftci *et al.* [58].

Elastic constants also quite differ for PBE+SOI and PBEsol+SOI as presented in Table 3. Other theoretical works are also not uniform in this matter.

Thanks to the excellent agreement with the bulk modulus, PBEsol+SOI+U is chosen as the accurate model for the description of mechanical properties. Thus for thorium monocarbide, predicted values are $c_{11} = 265$ GPa, $c_{22} = 85$ GPa and $c_{44} = 83$ GPa.

Calculated elastic constants of protactinium monocarbide using PBEsol+SOI+U also differ from calculated elastic constants of previous theoretical work [58] using PBE. The determined

values of elastic constants for protactinium monocarbide are $c_{11} = 378$ GPa, $c_{22} = 104$ GPa and $c_{44} = 86$ GPa.

### 4.2.3 Phonons

The actinide monocarbides are systems with two elements with significantly different atomic mass. A carbon is approximately 20 times lighter than an actinide element. As a result, a phonon spectrum is divided into a low-frequency phonons (acoustic branches) arising mainly from oscillations of heavy actinide atoms, and high-frequency phonons (optical branches) arising from oscillations of light carbon atoms. These bands are mostly separated by a frequency gap.

Fig. 10 presents partial phonon densities of states for PBE+SOI and PBEsol+SOI. While both approaches describe well phonon acoustic modes, comparison phonon spectra with experimental measured by the time-of-flight (TOF) technique [62] concludes that PBE+SOI greatly underestimates phonon optical modes. Same failure of PBE to reproduce optical branches is also well known for uranium monocarbide as discussed in Ref. [40].

Similarly, underestimated carbon phonon spectrum of PBE report Daroca et al. [53] and Sahoo et al. [54]. Their intensity peaks of optical branches are not consistent with experimental one [62].

It is assumed that the frequency gap presented in PBEsol+SOI result is missing in experiment [62] because of contamination of thorium monocarbide sample ($Th_{0.98}C_{0.96}N_{0.02}O_{0.02}$).

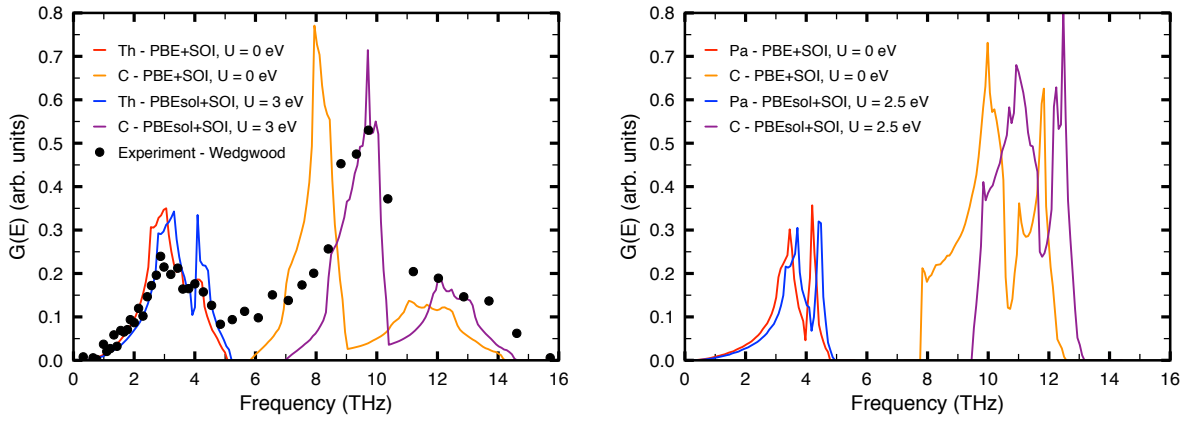


(a) ThC (b) PaC

Figure 10: Partial phonon densities of states G(E) for NaCl-type structure of actinide monocarbides. The TOF data (circles) are taken from Ref. [62].

The PBEsol+SOI approach is better in the reproduction of phonon density of states, as is the case of the Sommerfeld coefficient and the bulk modulus. Hence, all next calculations of lattice dynamics in this thesis are performed with PBEsol+SOI approach.

The same difference between optical branches at different approaches can be found for protactinium monocarbide as shown in Fig. 10. It can be expected from thorium monocarbide

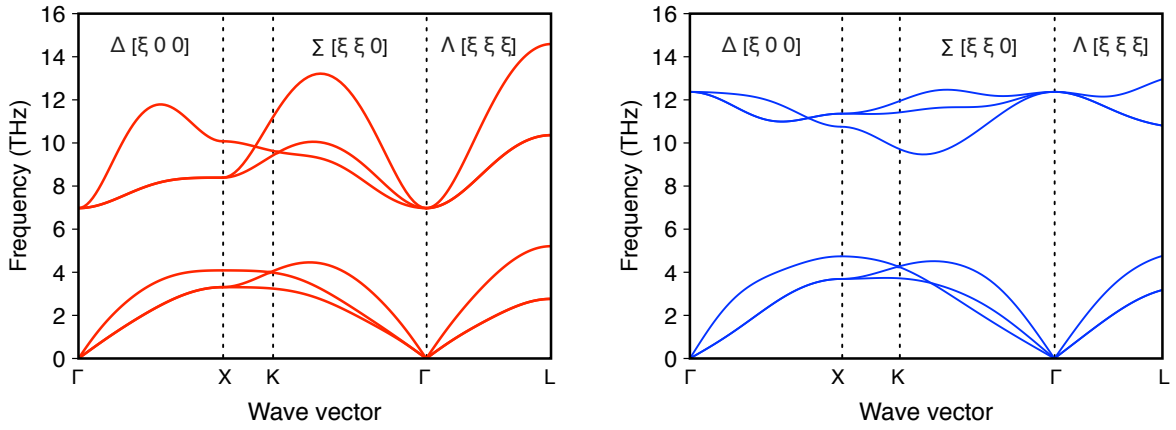


(a) ThC (b) PaC

Figure 11: Phonon dispersion relations of NaCl-type actinide monocarbides phonons.

analysis that the correct description of phonon density of states comes from the PBEsol+SOI approach and hence all next calculations of lattice dynamics in this thesis use this type of exchange-correlation pseudopotential.

Vibration spectra of thorium and protactinium atoms are very similar. However, the frequency gap of PaC is about 1 THz bigger than in ThC and carbon atom reaches 1 Thz higher frequency in ThC. Differences between those monocarbides stem from more dispersive optical branches of thorium monocarbide. The closer look provides Fig. 11 which illustrates dispersion relations of phonons in directions the $\Delta[\xi\ 0\ 0]$, $\sum[\xi\ \xi\ 0]$ and $\Lambda[\xi\ \xi\ \xi]$.

From the analysis of dispersion relation of ThC and PaC as shown in this thesis and dispersion relation of UC presented in Ref. [40] follows that increasing amount of occupied $5f$ states reduced dispersion of the optical branches.

As for the transverse branches, their degeneration is removed along $\sum[\xi\ \xi\ 0]$ direction in both actinide monocarbides.

Another property that confirms the accuracy of the PBEsol+SOI is a Debye temperature ($\theta_D$). Experimental measured Debye temperature of thorium monocarbide was determined as 262 K [56] and 280 K [55]. The calculated value of 249 K from PBEsol+SOI calculation is closer to experimental value than 229 K obtained from PBE+SOI calculation.

Generally, a phonon dynamics is governed by atomic force constants. The present results of atomic force constants of ThC calculated by PBE+SOI (PBEsol+SOI) amount to 160 (184) $Nm^{-1}$ for thorium and 67 (85) $Nm^{-1}$ for carbon.

The atomic force constants of protactinium monocarbide are expected to have higher values than for ThC based on elastic constants. As in thorium monocarbide, there is a significant difference between PBE+SOI and PBEsol+SOI approach. On-site force constants of the protactinium yield 202 (228) $Nm^{-1}$ and on-site force constant of carbon yield $\theta_C = 81$ (100) $Nm^{-1}$ using PBE+SOI (PBEsol+SOI) potencial.

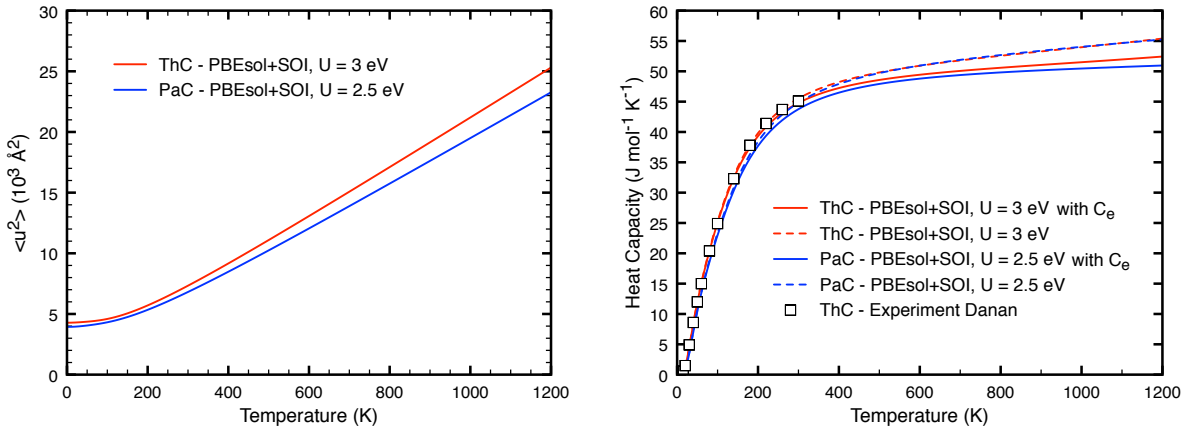


Figure 12: Calculated mean-square thermal atomic displacement versus temperature (left) and heat capacity at constant pressure as a functions of temperature for ThC and PaC (right). The experimental values of ThC are from Danan [56] (squares).

### 4.2.4 Thermodynamic properties

Thermodynamics properties are the most important properties for a design of nuclear fuels. Above all, it is heat capacity, thermal expansion and thermal conductivity. Calculation of thermal conductivity is beyond the scope of this thesis.

Mean square displacements in the direction [1 0 0] are shown in Fig. 12. Although both monocarbides have almost same the zero-point energy, they deviate due to unequal values of force constants with increasing temperature.

A heat capacity of a metal consists of two parts – atomic vibrations (phonons) and electronic contribution. Lattice vibrations dominate for all temperature range. The electronic part has an only weak effect on the total heat capacity at low temperature. However, with increasing temperature its importance increases and at common operating temperatures (1100-1200 K) in nuclear fuel cycle has negligible size. High heat capacity for nuclear fuel is required because it serves as protection against overheating and subsequent fuel melting. Thus, metallic materials are more desirable than insulators.

Fig. 12 illustrates the fast growth of both heat capacities at a constant pressure below room temperature. Around the room temperature, the growth trend is decreasing, and the increase in phonon thermal capacity is mainly driven by thermal expansion. Electronic heat capacities are much lower in comparison with thorium metal due to smaller metallic bonding in monocarbides.

Heat capacities of thorium and protactinium monocarbides are very similar. Although protactinium monocarbide has a lower phonon part, thanks to higher electronic, both capacities are almost identical at higher temperatures.

The accuracy of the calculated heat capacity at constant pressure of thorium monocarbide is verified by the excellent agreement with the experiment [56]. Another theoretical heat capacities

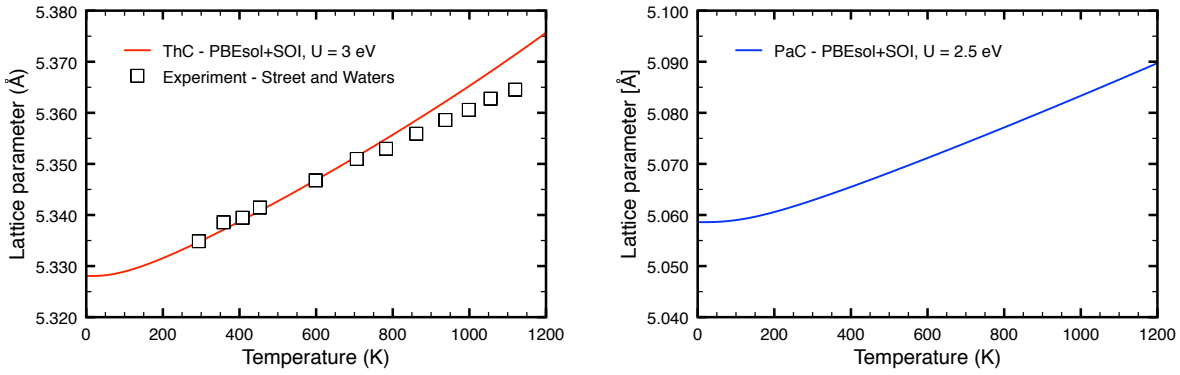


(a) ThC (b) PaC

Figure 13: Lattice constants versus temperature for actinide monocarbides. The experimental data (squares) are adopted from Ref. [63].

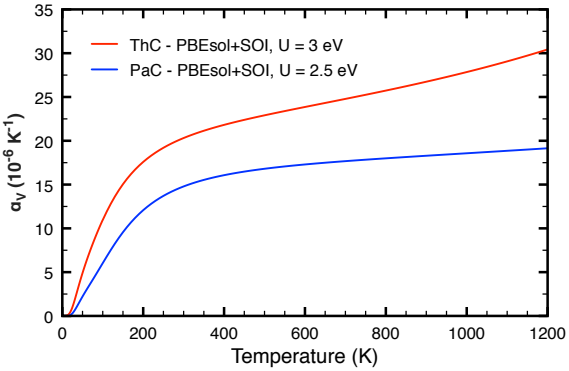


Figure 14: Volumetric thermal expansion coefficients versus temperature for NaCl-type thorium and protactinium monocarbides.

at constant pressure reported by Daroca et al. [53] and Sahoo et al. [54] slightly overestimate the experiment even though they do not include an electron contribution.

Due to lack of heat capacity experiment of protactinium monocarbide, the result presented here serves as a prediction.

It is also found the excellent match with the experiment changing of the lattice constant of ThC with temperature reported by Street and Waters [63], see Fig. 13. Comparison theoretical and experimental thermal expansion of thorium monocarbide indicates that the influence of high-order anharmonicity on thermodynamic properties becomes more prominent around 800 K.

The better comparison of thermal expansion between both monocarbides provides volumetric thermal expansion coefficients. From Fig. 14, it is clear that thorium monocarbide has a much higher thermal expansion than protactinium monocarbide. It means that internal energy $U(V)$ increases with volume change much faster in PaC than in ThC and therefore the gain of entropy from increasing volume of PaC is insufficient to compensate this change of internal energy $U(V)$ so fast as in ThC.

Volumetric thermal expansion coefficient yield $2.0 \cdot 10^{-5} K^{-1}$ at 300 K, similarly to reported values of $2.4 \cdot 10^{-5} K^{-1}$ by Daroca et al., Aydin et al., and $1.7 \cdot 10^{-5} K^{-1}$ by Sahoo et al.

Concerning PaC our result predicts $\alpha_V = 1.5 \cdot 10^{-5} K^{-1}$. Ciftci et al. determinate too high value of $\alpha_V = 2.2 \cdot 10^{-5} K^{-1}$ due to omittance of SOI and $5f$-states localizations.

# 5 Conclusion

Electronic, elastic, phonon and thermodynamic properties of thorium metal have been explored within the use of density functional theory calculations with respect to inclusion of spin-orbit interaction and varying on-site Coulomb interaction.

Although none of the effects influence the distribution of the density of states at the vicinity of Fermi energy ($E_F$), which is formed mainly by $6d$ and $5f$-states, both effects shift $6s$, $7s$ and $6p$-states to lower energy and stabilize the $fcc$ structure of Th.

Because of localization of $5f$-states tuned by Hubbard $U$ correlation ($U_{eff} = 1$ eV) and the inclusion of SOI, an accurate description of the elastic coefficient $c_{12}$, which previous theoretical works were not able to reproduce, is obtained. The inclusion of both effects is also needed for accurate description of bulk modulus, Sommerfeld coefficient, phonons density of states and dispersion relations, mean-square atomic displacement and thermal expansion.

On the other hand, properties as Debye temperature and heat capacity at a constant pressure are not sensitive to the inclusion of spin-orbit interaction.

Calculation omitting spin-orbit interaction cannot reproduce many properties mainly due to overestimation of lattice parameter in comparison of experiments. Thus, inclusion of spin-orbit interaction improves theoretical results indirectly because of reduction of lattice parameter as is shown in phonon dispersion relation of thorium metal.

The present DFT+U+SOI approach seems to be suitable for the precise description of the electronic structure and lattice dynamics of thorium metal and is therefore also used for thorium monocarbide as well as for protactinium monocarbide where the recorded data are scarce and only lattice parameter is known. Therefore, all the PaC results of this thesis serve as predictions.

Electronic densities of states of ThC a PaC thorium are very similar. However, the energy shift to lower energy based on stronger attractive Coulomb interaction and one extra electron in PaC electron configuration increases the amount of occupied 5 $f$-states. This compared to ThC significantly increases elastic coefficients $c_{11}$ and $c_{12}$, while $c_{44}$ remains the same.

Unlike thorium metal, PBEsol+SOI+U approximation for electron exchange and correlation effects is considered to be better to describe lattice dynamics than PBE+SOI+U due to the fact the phonon optical branches calculated by PBE+SOI+U are highly underestimated as in other theoretical works. Only by using PBEsol+SOI+U it is able to describe partial phonon density of states and Debye temperature of ThC in agreement with experiments.

While heat capacities of both monocarbides at a constant pressure are almost same, thermal expansion of ThC is significantly higher than PaC. The accuracy of presented heat capacity at a constant pressure and thermal expansion of ThC is verified by comparison with experiments.

As the main outcome in this thesis it follows that inclusion of spin-orbital interaction and an exact value of Hubbard $U$ potential is crucial for an accurate description of thermodynamic properties already in light actinides, not only in heavy actinides, what was the general view so far.

# References


[1] MANES, L. *Actinides - Chemistry and Physical Properties*. Berlin, Heidelberg: Springer-Verlag, 1985. ISBN 9783540390428.

[2] MORSS, L. R., N. M. EDELSTEIN, J. FUGER and J. J. KATZ. *The chemistry of the actinide and transactinide elements*. 3rd ed. Dordrecht: Springer, ©2006. ISBN 9781402035982.

[3] BLUNDELL, Stephen. *Magnetism in condensed matter*. Oxford: Oxford University Press, 2001. Oxford master series in condensed matter physics. ISBN 9780198505914.

[4] WILLS, J. M. and O. ERIKSSON. Actinide Ground-state Properties: Theoretical predictions. *Los Alamos Science*. 2000, **26**, 128-151.

[5] COTTON, Simon. *Lanthanide and actinide chemistry*. Chichester: Wiley, 2006. ISBN 9780470010082.

[6] CLARK, David L. The Chemical Complexities of Plutonium. *Los Alamos Science*. 2000, **26**, 364-381.

[7] ZWICKNAGL, G. and P. FULDE. The dual nature of 5f electrons and the origin of heavy fermions in U compounds. *Journal of Physics: Condensed Matter*. 2003, **15**(28), S1911-S1916. DOI: 10.1088/0953-8984/15/28/302. ISSN 09538984.

[8] DURAKIEWICZ, T., J. J. JOYCE, J. M. WILLS and C. D. BATISTA. Notes on the Dual Nature of 5f Electrons. *Journal of the Physical Society of Japan*. 2006, **75**(Suppl), 39-40. DOI: 10.1143/JPSJS.75S.39. ISSN 00319015.

[9] GREINER, J. D. and J. F. SMITH. Magnetic Susceptibility of High-Purity Thorium. *Physical Review B*. 1971, **4**(10), 3275-3277. DOI: 10.1103/PhysRevB.4.3275. ISSN 05562805.

[10] ABRAM, Tim and Sue ION. Generation-IV nuclear power: A review of the state of the science. *Energy Policy*. 2008, **36**(12), 4323-4330. DOI: 10.1016/j.enpol.2008.09.059. ISSN 03014215.

[11] INTERNATIONAL ATOMIC ENERGY AGENCY. *Thorium fuel cycle: potential benefits and challenges*. Vienna: International Atomic Energy Agency, 2005. ISBN 9201034059.

[12] JOHANSSON, B., R. AHUJA, O. ERIKSSON and J. M. WILLS. Anomalous fcc Crystal Structure of Thorium Metal. *Physical Review Letters*. 1995, **75**(2), 280-283. DOI: 10.1103/PhysRevLett.75.280. ISSN 00319007.

[13] MANARA, D., et. al. *Comprehensive nuclear materials*. Oxford: Elsevier Science, 2012. ISBN 9780080560274.

[14] WANG, C., et. al. Defect stability in thorium monocarbide: An ab initio study. *Chinese Physics B*. 2015, **24**(9), 097101-097106. DOI: 10.1088/1674-1056/24/9/097101. ISSN 16741056.

[15] VVEDENSKY, D. D. Quantum Theory of Electrons in Solids, London: The Blackett Laboratory, Imperial College, 2000-2001.

[16] HOLLAS, D., V. SVOBODA, O. SVOBODA and P. SLAVÍČEK. *Kvantová chemie: První čtení*. Praha: Slavíček a kol., 2014.

[17] BURKE, Kieron, et al. *The ABC of DFT*. Piscataway: Kieron Burke and friends, 2003.

[18] SLATER, J. C. Wave Functions in a Periodic Potential. *Physical Review*. 1937, **51**(10), 846-851. DOI: 10.1103/PhysRev.51.846. ISSN 0031899X.

[19] PAULI, Mark D. *Constructing the Muffin-Tin Potential* [online]. Milwaukee: University of Wisconsin, 1999. Available from: http://hermes.phys.uwm.edu/projects/elecstruct/mufpot/MP/MP.Theory4.html

[20] DUDAREV, S. L., et. al. Electron-energy-loss spectra and the structural stability of nickel oxide: An LSDA+U study. *Physical Review B*. 1998, **57**(3), 1505-1509. DOI: 10.1103/PhysRevB.57.1505. ISSN 01631829.

[21] FORSCHUNGSZENTRUM JÜLICH GMBH. Correlated electrons: from models to materials lecture notes of the Autumn School Correlated Electrons 2012 at Forschungszentrum Jülich, 3 - 7 September 2012. Jülich: Forschungszentrum Jülich, Zentralbibliothek, Verl, 2012. ISBN 9783893367962.

[22] CHAIKIN, P. M. and T. C. LUBENSKY. *Principles of condensed matter physics*. Cambridge [u.a.]: Cambridge Univ. Press, 2007. ISBN 9780521794503.

[23] KAXIRAS, Efthimios. *Atomic and electronic structure of solids*. New York: Cambridge University Press, 2003. ISBN 978-0521523394.

[24] GRIMVALL, Göran. *Thermophysical properties of materials*. Enl. and rev. ed. New York: Elsevier, 1999. ISBN 0444827943.

[25] LE PAGE, Y. and P. M. SAXE. Symmetry-general least-squares extraction of elastic data for strained materials from ab initio calculations of stress. *Physical Review B*. 2002, **65**(10), 104104-104117. DOI: 10.1103/PhysRevB.65.104104. ISSN 01631829.

[26] SOUBUSTA, Jan. *Fyzika pevných látek SLO/PL*. Olomouc: Univerzita Palackého v Olomouci, 2012. ISBN 9788024430959.

[27] TOGO, A. and I. TANAKA. First principles phonon calculations in materials science. *Scripta Materialia*. 2015, **108**, 1-5. DOI: 10.1016/j.scriptamat.2015.07.021. ISSN 13596462.

[28] KITTEL, Charles. *Úvod do fyziky pevných látek*. Praha: Academia, 1985.

[29] KRESSE, G. and J. FURTHMÜLLER. Efficient iterative schemes for ab initio total-energy calculations using a plane-wave basis set. *Physical Review B*. 1996, **54**(16), 11169-11186. DOI: 10.1103/PhysRevB.54.11169. ISSN 01631829.

[30] PERDEW, J. P., K. BURKE and M. ERNZERHOF. Generalized Gradient Approximation Made Simple. *Physical Review Letters*. 1996, **77**(18), 3865-3868. DOI: 10.1103/PhysRevLett.77.3865. ISSN 00319007.

[31] PERDEW, J. P., et. al. Restoring the Density-Gradient Expansion for Exchange in Solids and Surfaces. *Physical Review Letters*. 2008, **100**(13), 136406-136409. DOI: 10.1103/PhysRevLett.100.136406. ISSN 00319007.

[32] VINET, P., J. FERRANTE, J. H. ROSE and J. R. SMITH. Compressibility of solids. *Journal of Geophysical Research*. 1987, **92**(B9), 9319-9325. DOI: 10.1029/JB092iB09p09319. ISSN 01480227.

[33] SÖDERLIND, P., O. ERIKSSON, J. M. WILLS and A. M. BORING. Elastic constants of cubic f-electron elements: Theory. *Physical Review B*. 1993, **48**(13), 9306-9312. DOI: 10.1103/PhysRevB.48.9306. ISSN 01631829.

[34] SÖDERLIND, P., O. A. ERIKSSON, B. JOHANSSON and J. R. WILLS. Theoretical investigation of the high-pressure crystal structures of Ce and Th. *Physical Review B*. 1995, **52**(18), 13169-13176. DOI: 10.1103/PhysRevB.52.13169. ISSN 01631829.

[35] BOUCHET, J. and R. C. ALBERS. Elastic properties of the light actinides at high pressure. *Journal of Physics: Condensed Matter*. 2011, **23**(21), 215402-215408. DOI: 10.1088/0953-8984/23/21/215402. ISSN 09538984.

[36] GUPTA, S. C., K. D. JOSHI and S. BANERJEE. Experimental and Theoretical Investigations on d and f Electron Systems under High Pressure. *Metallurgical and Materials Transactions A*. 2008, **39**(7), 1593-1601. DOI: 10.1007/s11661-007-9377-1. ISSN 10735623.

[37] BARIA, J. K. and A. R. JANI. Lattice dynamics of La, Yb, Ce and Th. *Physica B: Condensed Matter*. 2010, **405**(8), 2065-2071. DOI: 10.1016/j.physb.2010.01.104. ISSN 09214526.

[38] HU, C., Z. ZENG, L. ZHANG, X. CHEN and L. CAI. Phase transition and thermodynamics of thorium from first-principles calculations. *Solid State Communications*. 2010, **150**(9-10), 393-398. DOI: 10.1016/j.ssc.2009.11.042. ISSN 00381098.

[39] JAROSZEWICZ, S., H. O. MOSCA and J. E. GARCÉS. The temperature behaviour of the elastic and thermodynamic properties of fcc thorium. *Journal of Nuclear Materials*. 2012, **429**(1-3), 136-142. DOI: 10.1016/j.jnucmat.2012.05.043. ISSN 00223115.

[40] WDOWIK, U. D., P. PIEKARZ, D. LEGUT and G. JAGŁO. Effect of spin-orbit and on-site Coulomb interactions on the electronic structure and lattice dynamics of uranium monocarbide. *Physical Review B*. 2016, **94**(5), 054303. DOI: 10.1103/PhysRevB.94.054303. ISSN 24699950.

[41] SCHMIDT, H. G. and G. WOLF. The heat capacity of Th and Th4H15 in the temperature range above 2 K. *Solid State Communications*. 1975, **16**(9), 1085-1087. DOI: 10.1016/0038-1098(75)90010-1. ISSN 00381098.

[42] GORDON, J. E., et. al. Superconductivity of Thorium and Uranium. *Physical Review*. 1966, **152**(1), 432-437. DOI: 10.1103/PhysRev.152.432. ISSN 0031899X.

[43] BAER, Y. and J. K. LANG. High-energy spectroscopic study of the occupied and unoccupied 5 f and valence states in Th and U metals. *Physical Review B*. 1980, **21**(6), 2060-2062. DOI: 10.1103/PhysRevB.21.2060. ISSN 01631829.

[44] GREINER, J. D. and J. F. SMITH. Magnetic Susceptibility of High-Purity Thorium. *Physical Review B*. 1971, **4**(10), 3275-3277. DOI: 10.1103/PhysRevB.4.3275. ISSN 05562805.

[45] ARMSTRONG, P. E., O. N. CARLSON and J. F. SMITH. Elastic Constants of Thorium Single Crystals in the Range 77–400 K. *Journal of Applied Physics*. 1959, **30**(1), 36-41. DOI: 10.1063/1.1734971. ISSN 00218979.

[46] REESE, R. A., S. K. SINHA and D. T. PETERSON. Phonon Spectrum of Thorium. *Physical Review B*. 1973, **8**(4), 1332-1337. DOI: 10.1103/PhysRevB.8.1332. ISSN 05562805.

[47] LAWSON, A. C., et. al. Melting of the light actinides. *Philosophical Magazine B*. 2009, **80**(1), 53-59. DOI: 10.1080/13642810008218339. ISSN 13642812.

[48] GRIFFEL, M. and R. E. SKOCHDOPOLE. The Heat Capacity and Entropy of Thorium from 18 to 300 K. *Journal of the American Chemical Society*. 1953, **75**(21), 5250-5251. DOI: 10.1021/ja01117a032. ISSN 00027863.

[49] NAKAMURA, J., Y. TAKAHASHI, S. IZUMI and M. KANNO. Heat capacity of metallic uranium and thorium from 80 to 1000 K. *Journal of Nuclear Materials*. 1980, **88**(1), 64-72. DOI: 10.1016/0022-3115(80)90386-4. ISSN 00223115.

[50] HERY, Y., A. WOJAKOWSK, M. BOIDRON and C. H. NOVION, Magnetic susceptibility of protactinium monocarbide. In: *2. International conference on the electronic structure of the actinides*: 13-16 September 1976. Wroclaw. 1976.

[51] SHEIN, I. R. and A. L. IVANOVSKIĬ. Effect of spin-orbit coupling on structural, electronic, and mechanical properties of cubic thorium monocarbide ThC. *Physics of the Solid State*. 2010, **52**(10), 2039-2043. DOI: 10.1134/S1063783410100069. ISSN 10637834.

[52] AYDIN, S., A. TATAR and Y. O. CIFTCI. A theoretical study for thorium monocarbide (ThC). *Journal of Nuclear Materials*. 2012, **429**(1-3), 55-69. DOI: 10.1016/j.jnucmat.2012.05.038. ISSN 00223115.

[53] PÉREZ DAROCA, D., S. JAROSZEWICZ, A. M. LLOIS and H. O. MOSCA. Phonon spectrum, mechanical and thermophysical properties of thorium carbide. *Journal of Nuclear Materials*. 2013, **437**(1-3), 135-138. DOI: 10.1016/j.jnucmat.2013.01.350. ISSN 00223115.

[54] SAHOO, B. D., K. D. JOSHI and S. C. GUPTA. Prediction of new high pressure structural sequence in thorium carbide: a first principles study. *Journal of Applied Physics*. 2015, **117**(18), 185903. DOI: 10.1063/1.4920929. ISSN 00218979.

[55] HARNESS, J. B., J. C. MATTHEWS and N MORTON. The specific heat of some uranium and thorium carbides between 1.8 K and 4.2 K. *British Journal of Applied Physics*. 1964, **15**(8), 963-966. DOI: 10.1088/0508-3443/15/8/313. ISSN 05083443.

[56] DANAN, J. Chaleur specifique de 2 a 300 K du monocarbure de thorium. Journal of Nuclear Materials. 1975, 57(3), 280-282. DOI: 10.1016/0022-3115(75)90211-1. ISSN 00223115.

[57] LORENZ, R., H. L. SCHERFF and N. TOUSSAINT. The carbothermic reduction of protactinium pentoxide and first results on protactinium carbide. *Journal of Inorganic and Nuclear Chemistry*. 1969, **31**(8), 2381-2390. DOI: 10.1016/0022-1902(69)80568-3. ISSN 00221902.

[58] ÇIFTCI, Y. Ö., et. al. The Structural, Elastic, Electronic, Thermodynamic and Vibrational Properties of Protactinium Monocarbide (PaC) from First-Principles Calculations. *Journal of Nanoelectronics and Optoelectronics*. 2016, **11**(4), 506-513. DOI: 10.1166/jno.2016.1915. ISSN 1555130X.

[59] GERWARD, L., J. S. OLSEN, U. BENEDICT and H. LUO. Compression of ThC to 50 GPa. *Journal of the Less Common Metals*. 1990, **161**(1), L11-L14. DOI: 10.1016/0022-5088(90)90330-M. ISSN 00225088.

[60] YU, Cun, et al. Structural Phase Transition of ThC Under High Pressure. *Scientific Reports*. 2017, **7**(1), 1-5. DOI: 10.1038/s41598-017-00226-4. ISSN 20452322.

[61] OLSEN, J. S., et. al. High-pressure structural studies of uranium and thorium compounds with the rocksalt structure. Physica. 1986, 139 &140B, 308-310. DOI: 10.1016/0378-4363(86)90584-X. ISSN 03784363.

[62] WEDGWOOD, F. A. Actinide chalcogenides and pnictides. III. Optical-phonon frequency determination in UX and ThX compounds by neutron scattering. *Journal of Physics C: Solid State Physics*. 1974, **7**(18), 3203-3218. DOI: 10.1088/0022-3719/7/18/006. ISSN 00223719.

[63] STREET, R. S. and T. N. WATERS, *The thermal expansion of ThC and ThN*. Atomic Energy Research Establishment: Harwell, 1962.

## Appendix: Radial Extent of 4f and 5f Valence Electrons

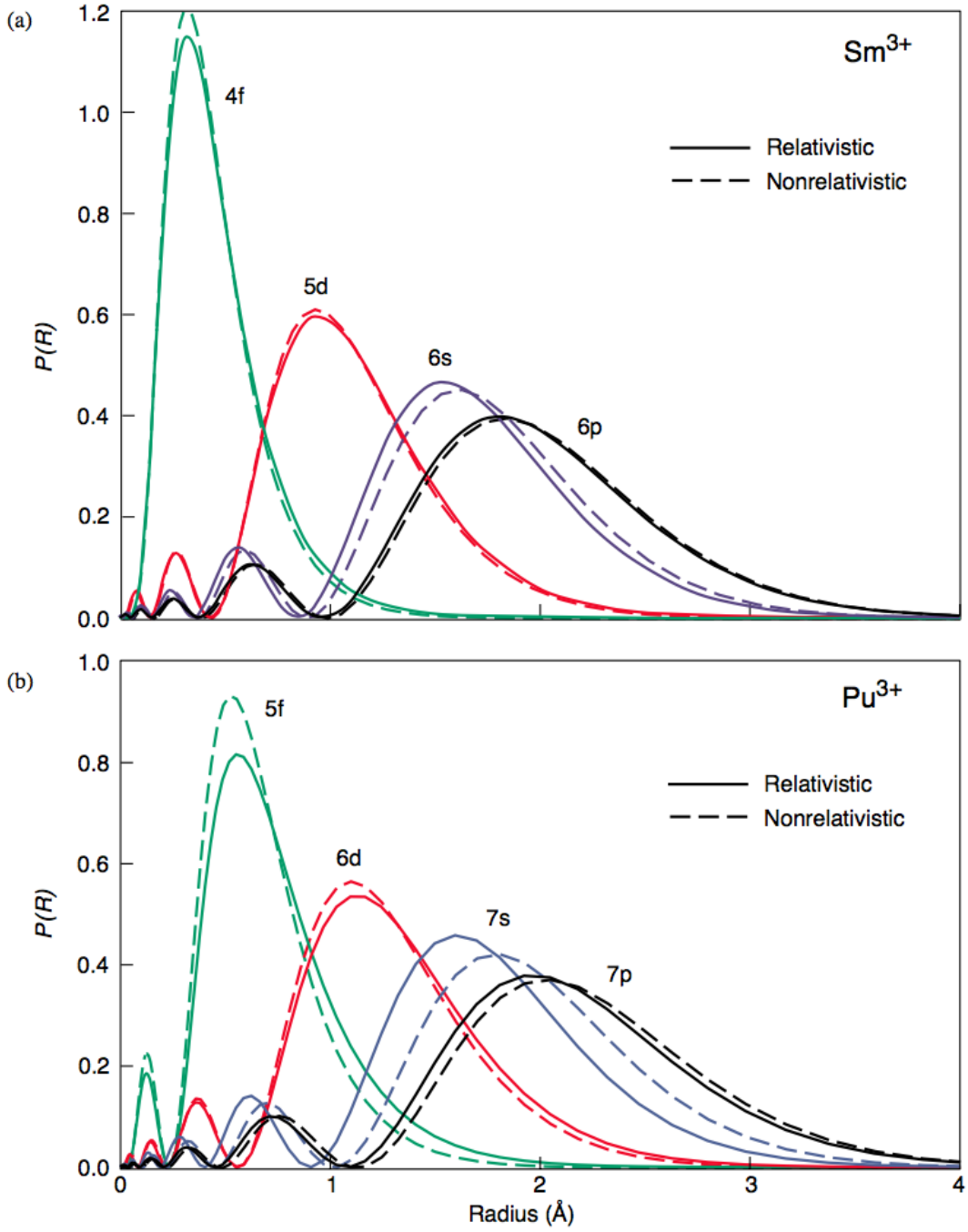


The radial probability $P(\vec{R}) = 4\pi r^2 R_{nl}^2$ of finding an electron at a distance $r$ from the nucleus is shown for:
a) the valence $4f$, $5d$, $6s$, and $6p$ orbitals of $Sm^{3+}$,
b) the valence $5f$, $6d$, $7s$, and $7p$ orbitals of $Pu^{3+}$.

## Acknowledgement

This bachelor thesis was supported by the European Regional Development Fund in the IT4Innovations national supercomputing center - Path to Exascale project, No. CZ.02.1.010.00.016_0130001791 within the Operational Programme Research Development and Education and by Czech Science Foundation project No. 17-27790S and Mobility grant No. 8x17046 by The Ministry of Education of the Czech Republic.